ELSEVIER

Available online at www.sciencedirect.com

SCIENCE DIRECT®

International Journal of Solids and Structures 43 (2006) 957–981

INTERNATIONAL JOURNAL OF SOLIDS and STRUCTURES

www.elsevier.com/locate/ijsolstr

On the singularities of the thermo-electro-elastic fields near the apex of a piezoelectric bonded wedge

Chung-De Chen *

Department of Structural Analysis, Aerospace Industrial Development Corporation, Taichung 407, Taiwan, ROC

Received 21 October 2004; received in revised form 4 March 2005
Available online 18 April 2005

Abstract

Based on the generalized Lekhnitskii formulation and Mellin transform, the thermo-electro-elastic fields of a piezoelectric bonded wedge are investigated in this paper. From the potential theory in a wedge-shaped region, a general form of the temperature change is proposed as a particular solution in the generalized Lekhnitskii formulation. The emphasis is on the singular behavior near the apex of the piezoelectric bonded wedge, including singularity orders and angular functions, which can be computed numerically. The interface between two materials can be either perfectly bonded, namely type A, so that the continuity of electric displacements holds, or a thin electrode, namely type B, so that the electric potential is grounded. Case studies of PZT-5H/PZT-4 and graphite-epoxy/PZT-4 bonded wedges reveal that, in most cases, the type B continuity condition has more severe singularities than type A due to the mixed boundary point of the electrostatics at the apex of the wedge. The results of this study show that the reduction or disappearance of singularity orders is possible through the appropriate selection of poling/fiber orientations and wedge angles.

Keywords: Piezoelectric; Wedge; Stress singularity; Thermal stress; Mellin transform

1. Introduction

Piezoelectric materials are widely used in actuators due to their electro-mechanical coupling behavior (Uchino, 1997). Polarized piezoceramics are among the most frequently used piezoelectric materials, usually being bonded to other materials. In many piezoelectric applications, the piezoceramics or fibrous reinforced composites are bonded together to form sharp corners or wedges, as shown in Fig. 1, resulting in

* Tel.: +886 4 27070001x503379; fax: +886 4 22842824.
E-mail address: chungdechen@ms.aidc.com.tw

0020-7683/$ - see front matter © 2005 Elsevier Ltd. All rights reserved.
doi:10.1016/j.ijsolstr.2005.03.011

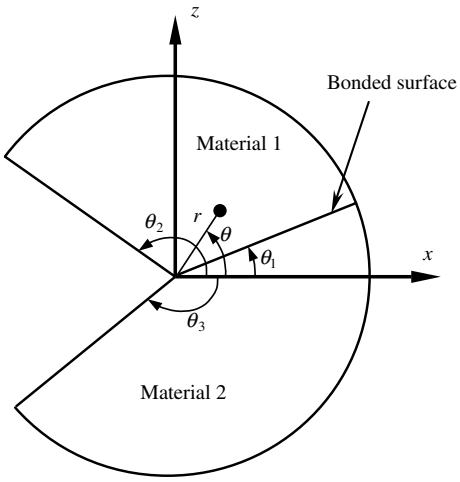

Fig. 1. The piezoelectric bonded wedge.

stress singularities due to geometric and material discontinuities. Because of the brittle properties of the piezoceramics and fibrous composites, the cracks frequently initiate from the apex of the wedges if the devices are operated in severe environments or under strenuous mechanical, electrical or thermal loading conditions.

Several mathematical tools, such as the eigenfunction expansion (Williams, 1952), Mellin transform (Bogy, 1968, 1972; Ma and Hour, 1989), complex potential functions (Theocaris, 1974; Delale, 1984; Chen and Nisitani, 1992; Chen, 1998; Chue and Liu, 2001) have been applied in solving the stress singularity orders in isotropic or anisotropic bonded wedges.

The thermal effects have also been investigated by the Mellin transform (Yang and Munz, 1994; Ma, 1995). These pioneering researchers found that the stress singularity orders are functions of wedge angles, material combinations and the boundary conditions at the edges. They are independent of the applied mechanical and thermal loadings and geometric conditions at more remote areas.

With regard to singular behavior in piezoelectric bonded wedges, few reports can be found in the available literature. Xu and Rajapakse (2000) used the generalized Lekhnitskii formulation (Lekhnitskii, 1963) associated with the eigenfunction expansion method to solve the in-plane singularity orders of a piezoelectric composite wedge or junction. Chue and Chen (2002) extended Xu and Rajapakse's approach to solve the stress singularities of a piezoelectric composite wedge under generalized plane deformation. The anti-plane singularities of a piezoelectric wedge were also investigated by the Mellin transform (Chue and Chen, 2003) and by eigenfunction expansion (Chen and Chue, 2003). The previous studies focused on piezoelectric wedges with perfect bonding, i.e., the tractions, displacements, normal components of electric displacements and electric potentials are continuous across the interface. In many piezoelectric applications, there exists a thin electrode between two piezoelectrics. The continuity conditions of the electrostatics fields are different for this type of wedge, and, until now, no research has been done on piezoelectric wedges with these kinds of continuity conditions.

In many applications of piezoelectric devices, thermal effects could be important because of the existences of a high temperature gradient and mismatch of thermal properties. Failures such as cracks could occur at high stress concentration locations. Some research has been done on thermal stresses of cracks in piezoelectric medium (Yu and Qin, 1996; Lu et al., 1998; Qin and Mai, 1999; Qin, 2001; Niraula and Noda, 2002; Shang et al., 2002, 2003). Theses studies revealed that the crack tips exhibit the conventional square root singularity. However, to the best of the author's knowledge, the thermal stresses in piezoelectric

wedges have never been investigated before. In this paper, the generalized Lekhnitskii formulation conjunction with the Mellin transform is used to study the thermo-piezoelectricity in the piezoelectric bonded wedge. The elastic and electrical boundary conditions at the edges are traction free and electrically insulated, respectively. Two types of continuity conditions across the interface are considered. The first case is that two piezoelectric materials are bonded perfectly while the second case is that there exists a thin electrode between two piezoelectric materials. Based on the potential theory with regard to the wedge-shaped region, a general form of the temperature change is put forward as a particular solution in the generalized Lekhnitskii formulation. Some reduced cases are compared with the existing literature to ensure the validity of the results. The results of this study provide practical information for designing more reliable piezoelectric devices.

2. Basic formulations

Consider a piezoelectric polarized in x–z plane. The constitute equations are

$$\begin{Bmatrix} \varepsilon_x \\ \varepsilon_y \\ \varepsilon_z \\ \gamma_{xz} \\ -E_x \\ -E_z \end{Bmatrix} = \begin{bmatrix} s_{11} & s_{12} & s_{13} & s_{14} & g_{11} & g_{31} \\ s_{12} & s_{22} & s_{23} & s_{24} & g_{12} & g_{32} \\ s_{13} & s_{23} & s_{33} & s_{34} & g_{13} & g_{33} \\ s_{14} & s_{24} & s_{34} & s_{44} & g_{14} & g_{34} \\ g_{11} & g_{12} & g_{13} & g_{14} & -\beta_{11} & -\beta_{13} \\ g_{31} & g_{32} & g_{33} & g_{34} & -\beta_{13} & -\beta_{33} \end{bmatrix} \begin{Bmatrix} \sigma_x \\ \sigma_y \\ \sigma_z \\ \tau_{xz} \\ D_x \\ D_z \end{Bmatrix} + \begin{Bmatrix} \alpha_1 \\ \alpha_2 \\ \alpha_3 \\ \alpha_4 \\ \lambda_1 \\ \lambda_3 \end{Bmatrix} T \tag{1.1}$$

$$\begin{Bmatrix} h_x \\ h_z \end{Bmatrix} = \begin{bmatrix} k_{11} & k_{13} \\ k_{13} & k_{33} \end{bmatrix} \begin{Bmatrix} H_x \\ H_z \end{Bmatrix} \tag{1.2}$$

where ε_{ij} and γ_{ij} are strains, σ_{ij} and τ_{ij} are stresses, E_i are electric fields, D_i are electric displacements, s_{ij} are elastic constants, g_{ij} are piezoelectric constants, β_{ij} are impermittivities, α_i are coefficients of thermal expansion, λ_i are pyroelectric constants, T is temperature change from a reference temperature, h_i are heat fluxes, H_i are heat intensities and k_{ij} are coefficients of heat conductivity. Using the concept of plane strain, the constitutive equations can be reduced to the form

$$\begin{Bmatrix} \varepsilon_x \\ \varepsilon_z \\ \gamma_{xz} \\ -E_x \\ -E_z \end{Bmatrix} = \begin{bmatrix} \tilde{s}_{11} & \tilde{s}_{13} & \tilde{s}_{14} & \tilde{g}_{11} & \tilde{g}_{31} \\ \tilde{s}_{13} & \tilde{s}_{33} & \tilde{s}_{34} & \tilde{g}_{13} & \tilde{g}_{33} \\ \tilde{s}_{14} & \tilde{s}_{34} & \tilde{s}_{44} & \tilde{g}_{14} & \tilde{g}_{34} \\ \tilde{g}_{11} & \tilde{g}_{13} & \tilde{g}_{14} & -\tilde{\beta}_{11} & -\tilde{\beta}_{13} \\ \tilde{g}_{31} & \tilde{g}_{33} & \tilde{g}_{34} & -\tilde{\beta}_{13} & -\tilde{\beta}_{33} \end{bmatrix} \begin{Bmatrix} \sigma_x \\ \sigma_z \\ \tau_{xz} \\ D_x \\ D_z \end{Bmatrix} + \begin{Bmatrix} \tilde{\alpha}_1 \\ \tilde{\alpha}_3 \\ \tilde{\alpha}_4 \\ \tilde{\lambda}_1 \\ \tilde{\lambda}_3 \end{Bmatrix} T \tag{2}$$

where

$$\tilde{s}_{ij} = s_{ij} - \frac{s_{i2}s_{j2}}{s_{22}} \tag{3.1}$$

$$\tilde{g}_{ij} = g_{ij} - \frac{s_{j2}g_{i2}}{s_{22}} \tag{3.2}$$

$$\tilde{\beta}_{ij} = \beta_{ij} + \frac{g_{i2}g_{j2}}{s_{22}} \tag{3.3}$$

$$\tilde{\alpha}_i = \alpha_i - \frac{s_{2i}\alpha_2}{s_{22}} \tag{3.4}$$

$$\tilde{\lambda}_i = \lambda_i - \frac{g_{i2}\alpha_2}{s_{22}} \tag{3.5}$$

The equilibrium equations, strain–displacements relations and compatibility relations are

$$\frac{\partial \sigma_x}{\partial x} + \frac{\partial \tau_{xz}}{\partial z} = 0 \tag{4.1}$$

$$\frac{\partial \tau_{xz}}{\partial x} + \frac{\partial \sigma_z}{\partial z} = 0 \tag{4.2}$$

$$\frac{\partial D_x}{\partial x} + \frac{\partial D_z}{\partial z} = 0 \tag{4.3}$$

$$\frac{\partial h_x}{\partial x} + \frac{\partial h_z}{\partial z} = 0 \tag{4.4}$$

$$\varepsilon_x = \frac{\partial u}{\partial x}, \quad \varepsilon_z = \frac{\partial w}{\partial z}, \quad \gamma_{xz} = \frac{\partial u}{\partial z} + \frac{\partial w}{\partial x} \tag{5.1}$$

$$E_x = -\frac{\partial \Phi}{\partial x}, \quad E_z = -\frac{\partial \Phi}{\partial z} \tag{5.2}$$

$$H_x = \frac{\partial T}{\partial x}, \quad H_z = \frac{\partial T}{\partial z} \tag{5.3}$$

$$\frac{\partial^2 \varepsilon_x}{\partial z^2} + \frac{\partial^2 \varepsilon_z}{\partial x^2} = \frac{\partial^2 \gamma_x}{\partial x \partial z} \tag{6.1}$$

$$\frac{\partial E_x}{\partial z} = \frac{\partial E_z}{\partial x} \tag{6.2}$$

$$\frac{\partial H_x}{\partial z} = \frac{\partial H_z}{\partial x} \tag{6.3}$$

where u, w are displacements, and Φ is electric potential.

Following the standard procedure of Lekhnitskii formulation (Lekhnitskii, 1963; Chue and Chen, 2002), we can introduce Airy's stress function F and the electric displacement function ϕ defined as

$$\sigma_x = \frac{\partial^2 F}{\partial z^2}, \quad \sigma_z = \frac{\partial^2 F}{\partial x^2}, \quad \tau_{xz} = -\frac{\partial^2 F}{\partial x \partial z}, \quad D_x = \frac{\partial \phi}{\partial z}, \quad D_z = -\frac{\partial \phi}{\partial x} \tag{7}$$

The governing equations of the thermo-piezoelectricity are

$$L_4 F + L_3 \phi = -\tilde{\alpha}_1 \frac{\partial^2 T}{\partial z^2} - \tilde{\alpha}_3 \frac{\partial^2 T}{\partial x^2} + \tilde{\alpha}_4 \frac{\partial^2 T}{\partial x \partial z} \tag{8.1}$$

$$L_3 F + L_2 \phi = \tilde{\lambda}_3 \frac{\partial T}{\partial x} - \tilde{\lambda}_1 \frac{\partial T}{\partial z} \tag{8.2}$$

where

$$L_4 = \tilde{s}_{33}\frac{\partial^4}{\partial x^4} - 2\tilde{s}_{34}\frac{\partial^4}{\partial x^3\partial z} + (2\tilde{s}_{13} + \tilde{s}_{44})\frac{\partial^4}{\partial x^2\partial z^2} - 2\tilde{s}_{14}\frac{\partial^4}{\partial x\partial z^3} + \tilde{s}_{11}\frac{\partial^4}{\partial z^4} \tag{9.1}$$

$$L_3 = -\tilde{g}_{33}\frac{\partial^3}{\partial x^3} + (\tilde{g}_{13} + \tilde{g}_{34})\frac{\partial^3}{\partial x^2\partial z} - (\tilde{g}_{31} + \tilde{g}_{14})\frac{\partial^3}{\partial x\partial z^2} + \tilde{g}_{11}\frac{\partial^3}{\partial z^3} \tag{9.2}$$

$$L_2 = -\tilde{\beta}_{33}\frac{\partial^2}{\partial x^2} + 2\tilde{\beta}_{13}\frac{\partial^2}{\partial x\partial z} - \tilde{\beta}_{11}\frac{\partial^2}{\partial z^2} \tag{9.3}$$

The general solutions of Eqs. (8) can be decomposed into homogeneous and particular solutions. The homogeneous solutions of the stresses and electric displacements can be expressed in terms of three analytic complex functions $f_1(z_1)$, $f_2(z_2)$ and $f_3(z_3)$, i.e.,

$$\sigma_{xh} = 2\mathrm{Re}[\mu_1^2 f_1'(z_1) + \mu_2^2 f_2'(z_2) + \mu_3^2\omega_3(\mu_3)f_3'(z_3)] \tag{10.1}$$

$$\sigma_{zh} = 2\mathrm{Re}[f_1'(z_1) + f_2'(z_2) + \omega_3(\mu_3)f_3'(z_3)] \tag{10.2}$$

$$\tau_{xzh} = -2\mathrm{Re}[\mu_1 f_1'(z_1) + \mu_2 f_2'(z_2) + \mu_3\omega_3(\mu_3)f_3'(z_3)] \tag{10.3}$$

$$D_{xh} = 2\mathrm{Re}[\mu_1\omega_1(\mu_1)f_1'(z_1) + \mu_2\omega_2(\mu_2)f_2'(z_2) + \mu_3 f_3'(z_3)] \tag{10.4}$$

$$D_{zh} = -2\mathrm{Re}[\omega_1(\mu_1)f_1'(z_1) + \omega_2(\mu_2)f_2'(z_2) + f_3'(z_3)] \tag{10.5}$$

where the subscript h denotes the homogeneous solutions and the prime denotes the derivative with respect to the argument,

$$\omega_1 = -\frac{l_3(\mu_1)}{l_2(\mu_1)}, \quad \omega_2 = -\frac{l_3(\mu_2)}{l_2(\mu_2)}, \quad \omega_3 = -\frac{l_3(\mu_3)}{l_4(\mu_3)} \tag{11}$$

$$z_i = x + \mu_i z \tag{12}$$

and μ_i are the roots of the following characteristic equation

$$l_4(\mu)l_2(\mu) - l_3^2(\mu) = 0 \tag{13}$$

with

$$l_4(\mu) = \tilde{s}_{11}\mu^4 - 2\tilde{s}_{14}\mu^3 + (2\tilde{s}_{13} + \tilde{s}_{44})\mu^2 - 2\tilde{s}_{34}\mu + \tilde{s}_{33} \tag{14.1}$$

$$l_3(\mu) = \tilde{g}_{11}\mu^3 - (\tilde{g}_{31} + \tilde{g}_{14})\mu^2 + (\tilde{g}_{13} + \tilde{g}_{34})\mu - \tilde{g}_{33} \tag{14.2}$$

$$l_2(\mu) = -\tilde{\beta}_{11}\mu^2 + 2\tilde{\beta}_{13}\mu - \tilde{\beta}_{33} \tag{14.3}$$

It can be shown that the six roots of μ are complex and distinct (Lekhnitskii, 1963). The homogenous solutions of displacements and electric potential are

$$u_h = 2\mathrm{Re}[a_1 f_1(z_1) + a_2 f_2(z_2) + a_3 f_3(z_3)] \tag{15.1}$$

$$w_h = 2\mathrm{Re}[b_1 f_1(z_1) + b_2 f_2(z_2) + b_3 f_3(z_3)] \tag{15.2}$$

$$\Phi_h = 2\mathrm{Re}[c_1 f_1(z_1) + c_2 f_2(z_2) + c_3 f_3(z_3)] \tag{15.3}$$

where

$$a_1 = \tilde{s}_{11}\mu_1^2 + \tilde{s}_{13} - \tilde{s}_{14}\mu_1 + \tilde{g}_{11}\mu_1\omega_1 - \tilde{g}_{31}\omega_1 \tag{16.1}$$

$$a_2 = \tilde{s}_{11}\mu_2^2 + \tilde{s}_{13} - \tilde{s}_{14}\mu_2 + \tilde{g}_{11}\mu_2\omega_2 - \tilde{g}_{31}\omega_2 \tag{16.2}$$

$$a_3 = \tilde{s}_{11}\mu_3^2\omega_3 + \tilde{s}_{13}\omega_3 - \tilde{s}_{14}\mu_3\omega_3 + \tilde{g}_{11}\mu_3 - \tilde{g}_{31} \tag{16.3}$$

$$b_1 = \tilde{s}_{13}\mu_1 + \frac{\tilde{s}_{33}}{\mu_1} - \tilde{s}_{34} + \tilde{g}_{13}\omega_1 - \frac{\tilde{g}_{33}\omega_1}{\mu_1} \tag{17.1}$$

$$b_2 = \tilde{s}_{13}\mu_2 + \frac{\tilde{s}_{33}}{\mu_2} - \tilde{s}_{34} + \tilde{g}_{13}\omega_2 - \frac{\tilde{g}_{33}\omega_2}{\mu_2} \tag{17.2}$$

$$b_3 = \tilde{s}_{13}\mu_3\omega_3 + \frac{\tilde{s}_{33}\omega_3}{\mu_3} - \tilde{s}_{34}\omega_3 + \tilde{g}_{13} - \frac{\tilde{g}_{33}}{\mu_2} \tag{17.3}$$

$$c_1 = \tilde{g}_{11}\mu_1^2 + \tilde{g}_{13} - \tilde{g}_{14}\mu_1 - \tilde{\beta}_{11}\mu_1\omega_1 + \tilde{\beta}_{13}\omega_1 \tag{18.1}$$

$$c_2 = \tilde{g}_{11}\mu_2^2 + \tilde{g}_{13} - \tilde{g}_{14}\mu_2 - \tilde{\beta}_{11}\mu_2\omega_2 + \tilde{\beta}_{13}\omega_2 \tag{18.2}$$

$$c_3 = \tilde{g}_{11}\mu_3^2\omega_3 + \tilde{g}_{13}\omega_3 - \tilde{g}_{14}\mu_3\omega_3 - \tilde{\beta}_{11}\mu_3 + \tilde{\beta}_{13} \tag{18.3}$$

The particular solutions depend on the heat conduction problem. From the basic equations (Eqs. (1.2), (4.4) and (5.3)), the governing equations for heat conduction are

$$k_{11}\frac{\partial^2 T}{\partial x^2} + 2k_{13}\frac{\partial^2 T}{\partial x \partial z} + k_{33}\frac{\partial^2 T}{\partial z^2} = 0 \tag{19}$$

We can introduce a complex function $f_p(z_p)$ related to the temperature change T as

$$T = 2\mathrm{Re}[f_p'(z_p)] \tag{20}$$

where the subscript p denotes the particular solution, and

$$z_p = x + \mu_p z \tag{21}$$

with μ_p the root of

$$k_{33}\mu^2 + 2k_{13}\mu + k_{11} = 0 \tag{22}$$

The particular solutions of the electro-elastic fields can be expressed as

$$\sigma_{xp} = 2\mathrm{Re}[\mu_p^2\zeta_1(\mu_p)f_p'(z_p)] \tag{23.1}$$

$$\sigma_{zp} = 2\mathrm{Re}[\zeta_1(\mu_p)f_p'(z_p)] \tag{23.2}$$

$$\tau_{xzp} = -2\mathrm{Re}[\mu_p\zeta_1(\mu_p)f_p'(z_p)] \tag{23.3}$$

$$D_{xp} = 2\mathrm{Re}[\mu_p\zeta_2(\mu_p)f_p'(z_p)] \tag{23.4}$$

$$D_{zp} = -2\mathrm{Re}[\zeta_2(\mu_p)f_p'(z_p)] \tag{23.5}$$

$$u_p = 2\mathrm{Re}[a_p f_p(z_p)] \tag{24.1}$$

$$w_p = 2\mathrm{Re}[b_p f_p(z_p)] \tag{24.2}$$

$$\Phi_p = 2\mathrm{Re}[c_p f_p(z_p)] \tag{24.3}$$

where

$$\zeta_1(\mu_p) = \frac{-l_1(\mu_p)l_3(\mu_p) + l_2(\mu_p)l_2^*(\mu_p)}{l_4(\mu_p)l_2(\mu_p) - l_3^2(\mu_p)} \tag{25.1}$$

$$\zeta_2(\mu_p) = \frac{l_4(\mu_p)l_1(\mu_p) - l_3(\mu_p)l_2^*(\mu_p)}{l_4(\mu_p)l_2(\mu_p) - l_3^2(\mu_p)} \tag{25.2}$$

$$a_p = \tilde{s}_{11}\mu_p^2\zeta_1 + \tilde{s}_{13}\zeta_1 - \tilde{s}_{14}\mu_p\zeta_1 + \tilde{g}_{11}\mu_p\zeta_2 - \tilde{g}_{31}\zeta_2 \tag{26.1}$$

$$b_p = \tilde{s}_{13}\mu_p\zeta_1 + \frac{\tilde{s}_{33}\zeta_1}{\mu_p} - \tilde{s}_{34}\zeta_1 + \tilde{g}_{13}\zeta_2 - \frac{\tilde{g}_{33}\zeta_2}{\mu_p} \tag{26.2}$$

$$c_p = \tilde{g}_{11}\mu_p^2\zeta_1 + \tilde{g}_{13}\zeta_1 - \tilde{g}_{14}\mu_p\zeta_1 - \tilde{\beta}_{11}\mu_p\zeta_2 + \tilde{\beta}_{13}\zeta_2 \tag{26.3}$$

In Eqs. (25), the polynomials $l_2^*(\mu)$ and $l_1(\mu)$ are

$$l_2^*(\mu) = -\tilde{\alpha}_1\mu^2 + \tilde{\alpha}_4\mu - \tilde{\alpha}_3 \tag{27.1}$$

$$l_1(\mu) = -\tilde{\lambda}_1\mu + \tilde{\lambda}_3 \tag{27.2}$$

The general solutions of electro-elastic fields are the combinations of Eqs. (10), (15), (24) and (25).

3. The Mellin transform solutions

The Mellin transform pairs of the electro-elastic fields are defined as

$$\hat{u}(s,\theta) = \int_0^\infty u(r,\theta)r^s\,\mathrm{d}r, \quad \hat{w}(s,\theta) = \int_0^\infty w(r,\theta)r^s\,\mathrm{d}r, \quad \hat{\Phi}(s,\theta) = \int_0^\infty \Phi(r,\theta)r^s\,\mathrm{d}r \tag{28.1}$$

$$u(r,\theta) = \frac{1}{2\pi\mathrm{i}}\int_{c-\mathrm{i}\infty}^{c+\mathrm{i}\infty}\hat{u}(s,\theta)r^{-s-1}\,\mathrm{d}s, \quad w(r,\theta) = \frac{1}{2\pi\mathrm{i}}\int_{c-\mathrm{i}\infty}^{c+\mathrm{i}\infty}\hat{w}(s,\theta)r^{-s-1}\,\mathrm{d}s$$
$$\Phi(r,\theta) = \frac{1}{2\pi\mathrm{i}}\int_{c-\mathrm{i}\infty}^{c+\mathrm{i}\infty}\hat{\Phi}(s,\theta)r^{-s-1}\,\mathrm{d}s \tag{28.2}$$

$$\hat{\sigma}_{ij}(s,\theta) = \int_0^\infty \sigma_{ij}(r,\theta)r^{s+1}\,\mathrm{d}r, \quad \hat{D}_i(s,\theta) = \int_0^\infty D_i(r,\theta)r^{s+1}\,\mathrm{d}r, \quad \hat{T}(s,\theta) = \int_0^\infty T(r,\theta)r^{s+1}\,\mathrm{d}r \tag{28.3}$$

$$\sigma_{ij}(r,\theta) = \frac{1}{2\pi\mathrm{i}}\int_{c-\mathrm{i}\infty}^{c+\mathrm{i}\infty}\hat{\sigma}_{ij}(s,\theta)r^{-s-2}\,\mathrm{d}s, \quad D_i(r,\theta) = \frac{1}{2\pi\mathrm{i}}\int_{c-\mathrm{i}\infty}^{c+\mathrm{i}\infty}\hat{D}_i(s,\theta)r^{-s-2}\,\mathrm{d}s,$$
$$T(r,\theta) = \frac{1}{2\pi\mathrm{i}}\int_{c-\mathrm{i}\infty}^{c+\mathrm{i}\infty}\hat{T}(s,\theta)r^{-s-2}\,\mathrm{d}s \tag{28.4}$$

where $(\hat{\bullet})$ denotes the Mellin transform of the quantity $(\bullet)$, s is the Mellin transform parameter and c is a real number which makes the inverse integral exist. The following regularity conditions hold

$$r^{s+2}\sigma_{ij}|_{r\to 0} = 0, \quad r^{s+1}u|_{r\to 0} = 0, \quad r^{s+1}w|_{r\to 0} = 0 \tag{29.1}$$

$$r^{s+2}\sigma_{ij}|_{r\to \infty} = 0, \quad r^{s+1}u|_{r\to \infty} = 0, \quad r^{s+1}w|_{r\to \infty} = 0 \tag{29.2}$$

$$r^{s+2}D_i|_{r\to 0}=0,\quad r^{s+1}\Phi|_{r\to 0}=0 \tag{30.1}$$

$$r^{s+2}D_i|_{r\to \infty}=0,\quad r^{s+1}\Phi|_{r\to \infty}=0 \tag{30.2}$$

In addition, with respect to a fixed θ, complex functions $\hat{f}_i(s)$ and $\hat{\bar{f}}_i(s)$ $(i=1,2,3,p)$ are defined as

$$\hat{f}_i(s)=\int_0^\infty f_i(z_i)z_i^s\,\mathrm{d}z_i \tag{31.1}$$

$$\hat{\bar{f}}_i(s)=\int_0^\infty \bar{f}_i(\bar{z}_i)\bar{z}_i^s\,\mathrm{d}\bar{z}_i \tag{31.2}$$

where the over-bar denotes the conjugate of the complex function. From the use of Eqs. (12), (21) and the integration by parts, Eqs. (31) become

$$\int_0^\infty f_i(z_i)r^s\,\mathrm{d}r=\frac{\hat{f}_i(s)}{\xi_i^{s+1}} \tag{32.1}$$

$$\int_0^\infty \bar{f}_i(\bar{z}_i)r^s\,\mathrm{d}r=\frac{\hat{\bar{f}}_i(s)}{\bar{\xi}_i^{s+1}} \tag{32.2}$$

$$\int_0^\infty f_i'(z_i)r^{s+1}\,\mathrm{d}r=-\frac{(s+1)\hat{f}_i(s)}{\xi_i^{s+2}} \tag{32.3}$$

$$\int_0^\infty \bar{f}_i'(\bar{z}_i)r^{s+1}\,\mathrm{d}r=-\frac{(s+1)\hat{\bar{f}}_i(s)}{\bar{\xi}_i^{s+2}} \tag{32.4}$$

where $x=r\cos\theta$, $y=r\sin\theta$ and $\xi_i=\cos\theta+\mathrm{i}\sin\theta$. In Eqs. (32.3) and (32.4), we have used the conditions that

$$z_i^{s+1}f_i(z_i)|_0^\infty=0 \tag{33.1}$$

$$\bar{z}_i^{s+1}\bar{f}_i(\bar{z}_i)|_0^\infty=0 \tag{33.2}$$

By using Eqs. (32), the Mellin transforms of the electro-elastic fields are

$$\hat{\sigma}_x=-(s+1)\left[\frac{\mu_1^2}{\xi_1^{s+2}}\hat{f}_1+\frac{\mu_2^2}{\xi_2^{s+2}}\hat{f}_2+\frac{\mu_3^2\omega_3}{\xi_3^{s+2}}\hat{f}_3+\frac{\mu_p^2\zeta_1}{\xi_p^{s+2}}\hat{f}_p+\frac{\bar{\mu}_1^2}{\bar{\xi}_1^{s+2}}\hat{\bar{f}}_1+\frac{\bar{\mu}_2^2}{\bar{\xi}_2^{s+2}}\hat{\bar{f}}_2+\frac{\bar{\mu}_3^2\bar{\omega}_3}{\bar{\xi}_3^{s+2}}\hat{\bar{f}}_3+\frac{\bar{\mu}_p^2\bar{\zeta}_1}{\bar{\xi}_p^{s+2}}\hat{\bar{f}}_p\right] \tag{34.1}$$

$$\hat{\sigma}_z=-(s+1)\left[\frac{1}{\xi_1^{s+2}}\hat{f}_1+\frac{1}{\xi_2^{s+2}}\hat{f}_2+\frac{\omega_3}{\xi_3^{s+2}}\hat{f}_3+\frac{\zeta_1}{\xi_p^{s+2}}\hat{f}_p+\frac{1}{\bar{\xi}_1^{s+2}}\hat{\bar{f}}_1+\frac{1}{\bar{\xi}_2^{s+2}}\hat{\bar{f}}_2+\frac{\bar{\omega}_3}{\bar{\xi}_3^{s+2}}\hat{\bar{f}}_3+\frac{\bar{\zeta}_1}{\bar{\xi}_p^{s+2}}\hat{\bar{f}}_p\right] \tag{34.2}$$

$$\hat{\tau}_{xz}=(s+1)\left[\frac{\mu_1}{\xi_1^{s+2}}\hat{f}_1+\frac{\mu_2}{\xi_2^{s+2}}\hat{f}_2+\frac{\mu_3\omega_3}{\xi_3^{s+2}}\hat{f}_3+\frac{\mu_p\zeta_1}{\xi_p^{s+2}}\hat{f}_p+\frac{\bar{\mu}_1}{\bar{\xi}_1^{s+2}}\hat{\bar{f}}_1+\frac{\bar{\mu}_2}{\bar{\xi}_2^{s+2}}\hat{\bar{f}}_2+\frac{\bar{\mu}_3\bar{\omega}_3}{\bar{\xi}_3^{s+2}}\hat{\bar{f}}_3+\frac{\bar{\mu}_p\bar{\zeta}_1}{\bar{\xi}_p^{s+2}}\hat{\bar{f}}_p\right] \tag{34.3}$$

$$\hat{D}_x=-(s+1)\left[\frac{\mu_1\omega_1}{\xi_1^{s+2}}\hat{f}_1+\frac{\mu_2\omega_2}{\xi_2^{s+2}}\hat{f}_2+\frac{\mu_3}{\xi_3^{s+2}}\hat{f}_3+\frac{\mu_p\zeta_2}{\xi_p^{s+2}}\hat{f}_p+\frac{\bar{\mu}_1\bar{\omega}_1}{\bar{\xi}_1^{s+2}}\hat{\bar{f}}_1+\frac{\bar{\mu}_2\bar{\omega}_2}{\bar{\xi}_2^{s+2}}\hat{\bar{f}}_2+\frac{\bar{\mu}_3}{\bar{\xi}_3^{s+2}}\hat{\bar{f}}_3+\frac{\bar{\mu}_p\bar{\zeta}_2}{\bar{\xi}_p^{s+2}}\hat{\bar{f}}_p\right] \tag{34.4}$$

$$\hat{D}_z = (s+1)\left[\frac{\omega_1}{\xi_1^{s+2}}\hat{f}_1 + \frac{\omega_2}{\xi_2^{s+2}}\hat{f}_2 + \frac{1}{\xi_3^{s+2}}\hat{f}_3 + \frac{\zeta_2}{\xi_p^{s+2}}\hat{f}_p + \frac{\bar{\omega}_1}{\bar{\xi}_1^{s+2}}\hat{\bar{f}}_1 + \frac{\bar{\omega}_2}{\bar{\xi}_2^{s+2}}\hat{\bar{f}}_2 + \frac{1}{\bar{\xi}_3^{s+2}}\hat{\bar{f}}_3 + \frac{\bar{\zeta}_2}{\bar{\xi}_p^{s+2}}\hat{\bar{f}}_p\right] \tag{34.5}$$

$$\hat{u} = \frac{a_1}{\xi_1^{s+1}}\hat{f}_1 + \frac{a_2}{\xi_2^{s+1}}\hat{f}_2 + \frac{a_3}{\xi_3^{s+1}}\hat{f}_3 + \frac{a_p}{\xi_p^{s+1}}\hat{f}_p + \frac{\bar{a}_1}{\bar{\xi}_1^{s+1}}\hat{\bar{f}}_1 + \frac{\bar{a}_2}{\bar{\xi}_2^{s+1}}\hat{\bar{f}}_2 + \frac{\bar{a}_3}{\bar{\xi}_3^{s+1}}\hat{\bar{f}}_3 + \frac{\bar{a}_p}{\bar{\xi}_p^{s+1}}\hat{\bar{f}}_p \tag{35.1}$$

$$\hat{w} = \frac{b_1}{\xi_1^{s+1}}\hat{f}_1 + \frac{b_2}{\xi_2^{s+1}}\hat{f}_2 + \frac{b_3}{\xi_3^{s+1}}\hat{f}_3 + \frac{b_p}{\xi_p^{s+1}}\hat{f}_p + \frac{\bar{b}_1}{\bar{\xi}_1^{s+1}}\hat{\bar{f}}_1 + \frac{\bar{b}_2}{\bar{\xi}_2^{s+1}}\hat{\bar{f}}_2 + \frac{\bar{b}_3}{\bar{\xi}_3^{s+1}}\hat{\bar{f}}_3 + \frac{\bar{b}_p}{\bar{\xi}_p^{s+1}}\hat{\bar{f}}_p \tag{35.2}$$

$$\hat{\Phi} = \frac{c_1}{\xi_1^{s+1}}\hat{f}_1 + \frac{c_2}{\xi_2^{s+1}}\hat{f}_2 + \frac{c_3}{\xi_3^{s+1}}\hat{f}_3 + \frac{c_p}{\xi_p^{s+1}}\hat{f}_p + \frac{\bar{c}_1}{\bar{\xi}_1^{s+1}}\hat{\bar{f}}_1 + \frac{\bar{c}_2}{\bar{\xi}_2^{s+1}}\hat{\bar{f}}_2 + \frac{\bar{c}_3}{\bar{\xi}_3^{s+1}}\hat{\bar{f}}_3 + \frac{\bar{c}_p}{\bar{\xi}_p^{s+1}}\hat{\bar{f}}_p \tag{35.3}$$

$$\hat{T} = -(s+1)\left[\frac{1}{\xi_p^{s+2}}\hat{f}_p + \frac{1}{\bar{\xi}_p^{s+2}}\hat{\bar{f}}_p\right] \tag{36}$$

The functions $\hat{f}_k(s)$ and $\hat{\bar{f}}_k(s)$, $k = 1,2,3$, remain unknowns.

4. Statement of problem

Consider a piezoelectric bonded wedge, as shown in Fig. 1. Two coordinate systems, x–z and r–θ coordinates, are used to define the wedge angles θ_1, θ_2 and θ_3 and the principal axes of materials. The orientations of the boundary edges are located at $\theta = \theta_2$ and θ_3 while the interface is at θ_1. Material 1 may be either piezoceramic or a fibrous-reinforced composite, while material 2 always refers to a piezoelectric. The poling and fiber orientation is in x–z plane and makes an angle β with z-axis as shown in Fig. 2. There is no piezoelectric coupling effect in the fibrous-reinforced composite. It is considered as a perfectly electric insulated body because of the assumption that it's impermittivity is much larger than the piezoceramic's. There is no electrostatics response inside the fibrous-reinforced composite so that it is modeled by the traditional Lekhnitskii formulation, i.e., only two analytic complex functions are required. The transformed solution has four unknown functions $\hat{f}_1(s)$, $\hat{f}_2(s)$, $\hat{\bar{f}}_1(s)$ and $\hat{\bar{f}}_2(s)$.

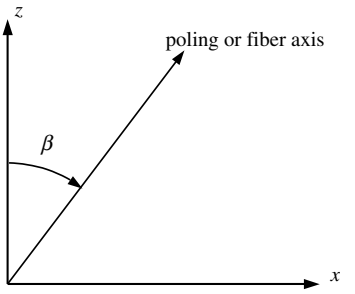

Fig. 2. The orientation of poling of piezoelectric or fiber of anisotropic composite.

The boundary edges of the piezoelectric are traction free and electrically insulated, i.e., at $\theta = \theta_2$ and $\theta = \theta_3$:

$$\sigma_{\mathrm{n}} = \sigma_x \sin^2\theta + \sigma_z \cos^2\theta - 2\tau_{xz} \sin\theta \cos\theta = 0 \tag{37.1}$$

$$\tau_{\mathrm{t}} = -\sigma_x \sin\theta \cos\theta + \sigma_z \sin\theta \cos\theta + \tau_{xz}(\cos^2\theta - \sin^2\theta) = 0 \tag{37.2}$$

$$D_{\mathrm{n}} = -D_x \sin\theta + D_z \cos\theta = 0 \tag{37.3}$$

where σ_{n} is the traction normal to the interface, τ_{t} is the traction tangential to the interface and D_{n} is the normal component of the electric displacement across the interface. If material 1 is a fibrous-reinforced composite, the boundary conditions at $\theta = \theta_2$ are Eqs. (37.1) and (37.2). At the interface, two types of continuity conditions, namely type A and B, are considered in this paper:

Type A: The two materials are perfectly bonded. For this type of boundary condition, the tractions, normal component of electric displacements, displacements and electric potential are continuous across the bonded surface, i.e., at $\theta = \theta_1$,

$$\sigma_{\mathrm{n}}^{(1)} = \sigma_{\mathrm{n}}^{(2)} \tag{38.1}$$

$$\tau_{\mathrm{t}}^{(1)} = \tau_{\mathrm{t}}^{(2)} \tag{38.2}$$

$$D_{\mathrm{n}}^{(1)} = D_{\mathrm{n}}^{(2)} \tag{38.3}$$

$$u^{(1)} = u^{(2)} \tag{38.4}$$

$$w^{(1)} = w^{(2)} \tag{38.5}$$

$$\Phi^{(1)} = \Phi^{(2)} \tag{38.6}$$

where the superscripts 1 and 2 denote materials 1 and 2, respectively. If material 1 is a fibrous-reinforced composite, the continuity conditions are Eqs. (38.1), (38.2), (38.4), (38.5) and

$$D_{\mathrm{n}}^{(2)} = 0 \tag{38.7}$$

Type B: A thin electrode exists between the two materials. The electrode is very thin so that it's thickness and stiffness can be ignored. For piezoelectric–piezoelectric bonded wedges, the tractions and displacements are continuous across the bonded surface and the electric potentials of the two materials are grounded at the interface, i.e., at $\theta = \theta_1$,

$$\sigma_{\mathrm{n}}^{(1)} = \sigma_{\mathrm{n}}^{(2)} \tag{39.1}$$

$$\tau_{\mathrm{t}}^{(1)} = \tau_{\mathrm{t}}^{(2)} \tag{39.2}$$

$$u^{(1)} = u^{(2)} \tag{39.3}$$

$$w^{(1)} = w^{(2)} \tag{39.4}$$

$$\Phi^{(1)} = 0 \tag{39.5}$$

$$\Phi^{(2)} = 0 \tag{39.6}$$

If material 1 is a fibrous-reinforced composite, the continuity conditions are Eqs. (39.1)–(39.4) and (39.6).

5. Procedure for the solution

Before going into the solution of the thermo-piezoelectricity, the temperature change T should first be investigated. Since the heat conduction problem is defined in a wedge-shaped region, it is reasonable to assume T to have the form

$$T = [1 - H(r - r_j)]r^{m_j}P_j(\Theta, m_j) + H(r - r_j)r^{n_j}Q_j(\Theta, n_j) \tag{40}$$

where the repeated index j indicates the summation, $H(r - r_j)$ is the Heaviside unit step function, m_j and n_j are the eigenvalues of the heat conduction wedge, P_j and Q_j are angular functions corresponding to m_j and n_j, respectively, and $\Theta = \theta - (\theta_2 - \theta_3)/2$. It should be noted that the 2-dimensional heat conduction problem can be correspondent to the antiplane problem in elasticity. Ma and Hour (1989) have proved that the antiplane stress singularity orders must be real in an anisotropic wedge. The same conclusion that both m_j and n_j are real can also be made. In addition, $P_j(\Theta, m_j)$ and $Q_j(\Theta, n_j)$ are integrable with respect to Θ on $[-(\theta_2 + \theta_3)/2, (\theta_2 + \theta_3)/2]$, so that for each m_j and n_j, they can expand by means of the Fourier series, i.e.,

$$\begin{aligned} T = {} & [1 - H(r - r_j)]r^{m_j}\left[a_{j0}(m_j) + a_{jk}(m_j)\cos\left(\frac{2k\pi\Theta}{\theta_2 + \theta_3}\right) + b_{jk}(m_j)\sin\left(\frac{2k\pi\Theta}{\theta_2 + \theta_3}\right)\right] \\ & + H(r - r_j)r^{n_j}\left[c_{j0}(n_j) + c_{jk}(n_j)\cos\left(\frac{2k\pi\Theta}{\theta_2 + \theta_3}\right) + d_{jk}(n_j)\sin\left(\frac{2k\pi\Theta}{\theta_2 + \theta_3}\right)\right] \end{aligned} \tag{41}$$

where a_{jk}, b_{jk}, c_{jk} and d_{jk} are coefficients of the Fourier series. Therefore, the complex function $f'_p(z_p)$ can be written as

$$\begin{aligned} f'_p = {} & [1 - H(r - r_j)]r^{m_j}\left[A_{j0} + A_{jk}\cos\left(\frac{2k\pi\Theta}{\theta_2 + \theta_3}\right) + B_{ik}\sin\left(\frac{2k\pi\Theta}{\theta_2 + \theta_3}\right)\right] \\ & + H(r - r_j)r^{n_j}\left[C_{j0} + C_{jk}\cos\left(\frac{2k\pi\Theta}{\theta_2 + \theta_3}\right) + D_{ik}\sin\left(\frac{2k\pi\Theta}{\theta_2 + \theta_3}\right)\right] \end{aligned} \tag{42}$$

where A_{jk}, B_{jk}, C_{jk}, D_{jk} are complex functions and

$$2\mathrm{Re}[A_{jk}] = a_{jk}, \quad 2\mathrm{Re}[B_{jk}] = b_{jk}, \quad 2\mathrm{Re}[C_{jk}] = c_{jk}, \quad 2\mathrm{Re}[D_{jk}] = d_{ik} \tag{43}$$

The combination of Eqs. (32) and (42) yields

$$\begin{aligned} \hat{f}_p(s) = {} & -\frac{\xi_p^{s+2}r_j^{m_j+s+2}}{(s+1)(m_j+s+2)}\left[A_{j0} + A_{jk}\cos\left(\frac{2k\pi\Theta}{\theta_2 + \theta_3}\right) + B_{jk}\sin\left(\frac{2k\pi\Theta}{\theta_2 + \theta_3}\right)\right] \\ & + \frac{\xi_p^{s+2}r_j^{n_j+s+2}}{(s+1)(n_j+s+2)}\left[C_{j0} + C_{jk}\cos\left(\frac{2k\pi\Theta}{\theta_2 + \theta_3}\right) + D_{jk}\sin\left(\frac{2k\pi\Theta}{\theta_2 + \theta_3}\right)\right] \end{aligned} \tag{44.1}$$

$$\begin{aligned} \hat{\bar{f}}_p(s) = {} & -\frac{\bar{\xi}_p^{s+2}r_j^{m_j+s+2}}{(s+1)(m_j+s+2)}\left[\overline{A}_{j0} + \overline{A}_{jk}\cos\left(\frac{2k\pi\Theta}{\theta_2 + \theta_3}\right) + \overline{B}_{jk}\sin\left(\frac{2k\pi\Theta}{\theta_2 + \theta_3}\right)\right] \\ & + \frac{\bar{\xi}_p^{s+2}r_j^{n_j+s+2}}{(s+1)(n_j+s+2)}\left[\overline{C}_{j0} + \overline{C}_{jk}\cos\left(\frac{2k\pi\Theta}{\theta_2 + \theta_3}\right) + \overline{D}_{jk}\sin\left(\frac{2k\pi\Theta}{\theta_2 + \theta_3}\right)\right] \end{aligned} \tag{44.2}$$

In Eqs. (44), the following two conditions:

$$\mathrm{Re}[m_j + s + 2] > 0 \tag{45.1}$$

$$\mathrm{Re}[n_j + s + 2] < 0 \tag{45.2}$$

must be hold for the existence of the Mellin transform.

For the temperature field under a specific heat conduction problem in a piezoelectric wedge, it is crucial to determine the coefficients A_{jk}, B_{jk}, C_{jk} and D_{jk}. For example, consider a specific temperature field

$$T = T_0[1 - H(r - r_0)] \tag{46}$$

Eq. (46), which was used to determine the regular stress term of an isotropic bonded wedge (Yang and Munz, 1994), can be obtained from Eq. (42) by setting $k = j = 0$, $m_0 = 0$, $A_{j0} = T_0/2$ and $C_{jk} = D_{jk} = 0$. Then Eqs. (44) become

$$\hat{f}_p(s) = -\frac{T_0 \xi_p^{s+2} r_0^{s+2}}{2(s+1)(s+2)} \tag{47.1}$$

$$\hat{\bar{f}}_p(s) = -\frac{T_0 \bar{\xi}_p^{s+2} r_0^{s+2}}{2(s+1)(s+2)} \tag{47.2}$$

Once $\hat{f}_p(s)$ and $\hat{\bar{f}}_p(s)$ are assigned, the simultaneous equations in matrix form

$$\mathbf{Mf} = \mathbf{f_p} \tag{48}$$

can be obtained by substituting Eqs. (34) and (35) into the boundary conditions (Eqs. (37)) and continuity conditions (Eqs. (38) for type A or Eqs. (39) for type B). In Eq. (48), the matrix $\mathbf{M}$ consists of the material properties, wedge angles and the Mellin transformed parameter s. The dimension of $\mathbf{M}$ is 12×12 for piezoelectric–piezoelectric bonded wedge and 10×10 for composite–piezoelectric bonded wedge. The vector $\mathbf{f_p}$ consists of the particular terms $\hat{f}_p(s)$ and $\hat{\bar{f}}_p(s)$. The form of the vector $\mathbf{f}$ is

$$\mathbf{f} = \left[\hat{f}_1^{(1)} \quad \hat{f}_2^{(1)} \quad \hat{f}_3^{(1)} \quad \hat{\bar{f}}_1^{(1)} \quad \hat{\bar{f}}_2^{(1)} \quad \hat{\bar{f}}_3^{(1)} \quad \hat{f}_1^{(2)} \quad \hat{f}_2^{(2)} \quad \hat{f}_3^{(2)} \quad \hat{\bar{f}}_1^{(2)} \quad \hat{\bar{f}}_2^{(2)} \quad \hat{\bar{f}}_3^{(2)} \right]^t \tag{49.1}$$

for piezoelectric–piezoelectric bonded wedges and

$$\mathbf{f} = \left[\hat{f}_1^{(1)} \quad \hat{f}_2^{(1)} \quad \hat{\bar{f}}_1^{(1)} \quad \hat{\bar{f}}_2^{(1)} \quad \hat{f}_1^{(2)} \quad \hat{f}_2^{(2)} \quad \hat{f}_3^{(2)} \quad \hat{\bar{f}}_1^{(2)} \quad \hat{\bar{f}}_2^{(2)} \quad \hat{\bar{f}}_3^{(2)} \right]^t \tag{49.2}$$

for composite–piezoelectric bonded wedges. In Eqs. (49), t denotes transpose of the vector. For general purposes, the following derivation is for the case of piezoelectric–piezoelectric bonded wedges. Based on Cramer's rule, the solutions of Eq. (48) can be obtained and the transformed electro-elastic fields can be expressed as

$$\hat{\sigma}_{ij}^{(k)}(s,\theta) = \frac{s+1}{D(s)} F_{ij}^{(k)}(s,\theta) \tag{50.1}$$

$$\hat{D}_i^{(k)}(s,\theta) = \frac{s+1}{D(s)} G_i^{(k)}(s,\theta) \tag{50.2}$$

where $D(s)$ is the determinant of the matrix $\mathbf{M}$ and the superscript $k = 1, 2$ denote the kth material. In Eqs. (50), the exact forms of the functions $F_{ij}^{(k)}(s,\theta)$ and $G_i^{(k)}(s,\theta)$ are difficult to obtain. They can be computed by numerical methods. The stresses and electric displacements can be obtained by applying Mellin inverse transform to Eqs. (50). Before calculating the Mellin inverse integral, we first define the inverse integral path parameter c. By knowing the poles of Eqs. (50), i.e., the zeros of $D(s)$, the inverse transform can be investigated by the residue theorem. Assume that the displacements and stresses have the following forms:

$$u, w \propto r^{-s'-1} \tag{51.1}$$

$$\sigma_{ij} \propto r^{-s'-2} \tag{51.2}$$

where s' is a complex number. From the regularity conditions of Mellin transform (see Eqs. (29) and (30)), we have

$$r \to 0, \quad c > \mathrm{Re}[s'] \tag{52.1}$$

$$r \to \infty, \quad c < \mathrm{Re}[s'] \tag{52.2}$$

where $c = \mathrm{Re}[s]$. Also, from the assumption of finite values of displacements when $r \to 0$ and $r \to \infty$, we have

$$r \to 0, \quad \mathrm{Re}[s'] < -1 \tag{53.1}$$

$$r \to \infty, \quad \mathrm{Re}[s'] > -1 \tag{53.2}$$

The application of the residue theorem implies that the parameter s' is the zero of $D(s)$. Denote the zeros of $D(s)$ located in the half planes $\mathrm{Re}[s] < -1$ and $\mathrm{Re}[s] > -1$ be s_k and $\tilde{s}_k$ $(k = 1, 2, \ldots)$, respectively, and $\mathrm{Re}[s_k] > \mathrm{Re}[s_{k+1}]$, $\mathrm{Re}[\tilde{s}_k] < \mathrm{Re}[\tilde{s}_{k+1}]$. From the calculations in Eqs. (52) and (53), the inverse integral path Γ should lie in the regularity strip $\mathrm{Re}[s_1] < \mathrm{Re}[s] < \mathrm{Re}[\tilde{s}_1]$ as shown in Fig. 3.

The main focus of this study is the thermo-electro-elastic behavior when $r \to 0$, for which the inverse integral path is shown in Fig. 4. In Fig. 4, the path Γ_1 is a semi-circle with infinite radius. It can be shown that the integrals along path Γ_1 are identically zero. From the residue theorem, the thermo-electro-elastic fields for $r \to 0$ can be written as

$$\sigma_{ij}(r, \theta) = \sum_k \mathrm{Re}s[\hat{\sigma}_{ij}(s, \theta) r^{-s-2}; s_k] \tag{54.1}$$

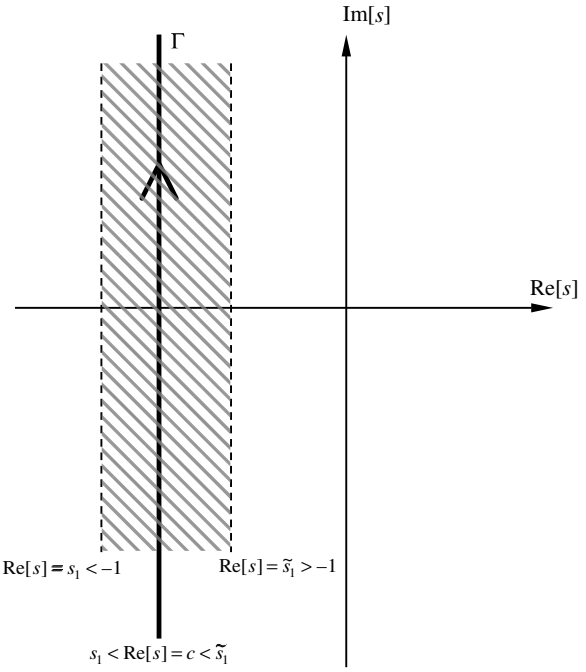

Fig. 3. The path of the inverse transform integral Γ.

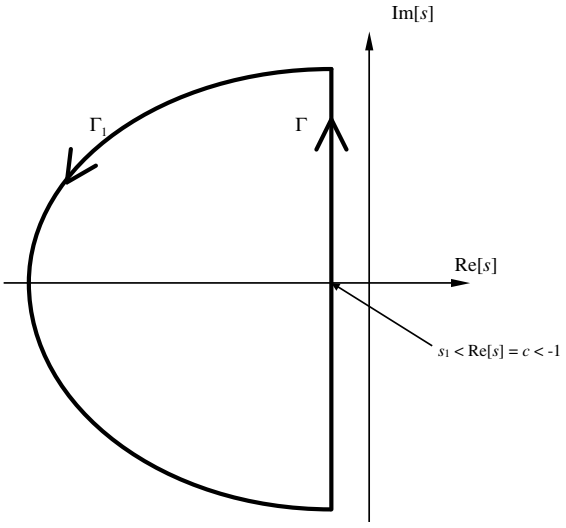

Fig. 4. The path of the inverse transform for $r \to 0$.

$$D_i(r,\theta) = \sum_k \mathrm{Re}\, s[\hat{D}_i(s,\theta) r^{-s-2};\, s_k] \tag{54.2}$$

For a specific eigenvalue m_j of the heat conduction wedge, the number of poles s_k in Eqs. (54) is finite due to Eqs. (45.1) and (53.1). However, in general cases, there are infinite numbers of m_j and each $m_j \geqslant 0$ for finite values of the temperature at the apex of the wedge. From the superposition principle, there are infinite numbers of s_k. The stresses become singular if the zeros are in the interval $-2 < \mathrm{Re}[s]$ and the singularity order is defined as $(-s-2)$. Also from Eq. (53.1), the singularity orders can be computed numerically by finding the zeros of $D(s)$ in the open strip $-2 < \mathrm{Re}[s] < -1$.

In the most cases, s_k are simple poles of $\hat{\sigma}_{ij}$ or $\hat{D}_i$. For the first eigenvalue s_1, the singular thermo-electro-elastic fields are

$$\sigma_{ij}^{(k)}(r,\theta) = \lim_{s\to s_1}[\hat{\sigma}_{ij}^{(k)}(s,\theta) r^{-s-2}(s-s_1)] = K^{\sigma} r^{-s_1-2} f_{ij}^{(k)}(\theta) \tag{55.1}$$

$$D_i^{(k)}(r,\theta) = \lim_{s\to s_1}[\hat{D}_i^{(k)}(s,\theta) r^{-s-2}(s-s_1)] = K^{D} r^{-s_1-2} g_i^{(k)}(\theta) \tag{55.2}$$

for real s_1 and

$$\begin{aligned}\sigma_{ij}^{(k)}(r,\theta) &= \lim_{s\to s_1}[\hat{\sigma}_{ij}^{(k)}(s,\theta) r^{-s-2}(s-s_1)] + \lim_{s\to \bar{s}_1}[\hat{\sigma}_{ij}^{(k)}(s,\theta) r^{-s-2}(s-\bar{s}_1)] \\ &= r^{-p_1-2}\Big\{\Big[\cos(q_1 \ln r) f_{ijc}^{(k)}(\theta) + \sin(q_1 \ln r) f_{ijs}^{(k)}(\theta)\Big] K_{\mathrm{Re}}^{\sigma} \\ &\quad + \Big[\cos(q_1 \ln r) f_{ijs}^{(k)}(\theta) - \sin(q_1 \ln r) f_{ijc}^{(k)}(\theta)\Big] K_{\mathrm{Im}}^{\sigma}\Big\}\end{aligned} \tag{56.1}$$

$$\begin{aligned}D_i^{(k)}(r,\theta) &= \lim_{s\to s_1}\left[\hat{D}_{ij}^{(k)}(s,\theta) r^{-s-2}(s-s_1)\right] + \lim_{s\to \bar{s}_1}\left[\hat{D}_{ij}^{(k)}(s,\theta) r^{-s-2}(s-\bar{s}_1)\right] \\ &= r^{-p_1-2}\Big\{\Big[\cos(q_1 \ln r) g_{ic}^{(k)}(\theta) + \sin(q_1 \ln r) g_{is}^{(k)}(\theta)\Big] K_{\mathrm{Re}}^{D} \\ &\quad + \Big[\cos(q_1 \ln r) g_{is}^{(k)}(\theta) - \sin(q_1 \ln r) g_{ic}^{(k)}(\theta)\Big] K_{\mathrm{Im}}^{D}\Big\}\end{aligned} \tag{56.2}$$

for complex $s_1 = p_1 i q_1$ with real p_1 and q_1. In Eqs. (55) and (56), K^{σ} and K^{D}, K^{σ}_{Re}, K^{σ}_{Im}, K^{D}_{Re} and K^{D}_{Im} are intensity factors and $f^{(k)}_{ij}(\theta)$, $g^{(k)}_{i}(\theta)$, $f^{(k)}_{ijc}(\theta)$, $f^{(k)}_{ijs}(\theta)$, $g^{(k)}_{ic}(\theta)$ and $g^{(k)}_{is}(\theta)$ are angular functions. Define

$$f_{\theta\theta}(\theta_1) = f_{\theta\theta c}(\theta_1) = g_{\theta}(\theta_1) = g_{\theta c}(\theta_1) = 1 \tag{57.1}$$

$$f_{\theta\theta s}(\theta_1) = g_{\theta s}(\theta_1) = 0 \tag{57.2}$$

for piezoelectric/piezoelectric and type B of composite/piezoelectric bonded wedges, and

$$f_{\theta\theta}(\theta_1) = f_{\theta\theta c}(\theta_1) = g_{\theta}(\theta_4) = g_{\theta c}(\theta_4) = 1 \tag{57.3}$$

$$f_{\theta\theta s}(\theta_1) = g_{\theta s}(\theta_4) = 0 \tag{57.4}$$

for type A of composite/piezoelectric bonded wedge, where $\theta_4 = (\theta_1 - \theta_3)/2$.

6. Numerical results and discussion

The material properties considered in this study are given below:

PZT5H with z-axis polarization (Shang and Kuna, 2003):

$$s_{11} = s_{22} = 10.055 \times 10^{-12}\ \mathrm{m^2/N}, \quad s_{33} = 7.1163 \times 10^{-12}\ \mathrm{m^2/N},$$
$$s_{12} = -4.0295 \times 10^{-12}\ \mathrm{m^2/N}, \quad s_{13} = s_{23} = -1.5694 \times 10^{-12}\ \mathrm{m^2/N},$$
$$s_{44} = 18.369 \times 10^{-12}\ \mathrm{m^2/N}, \quad s_{14} = s_{24} = s_{34} = 0,$$
$$g_{14} = 20.681 \times 10^{-3}\ \mathrm{V\,m/N}, \quad g_{31} = g_{32} = -5.8256 \times 10^{-3}\ \mathrm{V\,m/N},$$
$$g_{33} = 14.324 \times 10^{-3}\ \mathrm{V\,m/N}, \quad g_{11} = g_{12} = g_{13} = g_{34} = 0,$$
$$\beta_{11} = 4.2943 \times 10^{7}\ \mathrm{V^2/N}, \quad \beta_{33} = 4.5425 \times 10^{7}\ \mathrm{V^2/N}, \quad \beta_{13} = 0,$$
$$\alpha_1 = \alpha_2 = 9.6384 \times 10^{-6}\ \mathrm{K^{-1}}, \quad \alpha_3 = 3.9634 \times 10^{-6}\ \mathrm{K^{-1}}, \quad \alpha_4 = 0,$$
$$\lambda_3 = 2956.5\ \mathrm{N\,C^{-1}\,K^{-1}}, \quad \lambda_1 = 0,$$
$$k_{11} = 50\ \mathrm{W\,K^{-1}\,m^{-1}}, \quad k_{33} = 75\ \mathrm{W\,K^{-1}\,m^{-1}}, \quad k_{13} = 0$$

PZT-4 with z-axis polarization (Berlincourt et al., 1964; Ding et al., 2003):

$$s_{11} = s_{22} = 10.9 \times 10^{-12}\ \mathrm{m^2/N}, \quad s_{33} = 7.9 \times 10^{-12}\ \mathrm{m^2/N}, \quad s_{12} = -5.42 \times 10^{-12}\ \mathrm{m^2/N},$$
$$s_{13} = s_{23} = -2.1 \times 10^{-12}\ \mathrm{m^2/N}, \quad s_{44} = 19.3 \times 10^{-12}\ \mathrm{m^2/N}, \quad s_{14} = s_{24} = s_{34} = 0,$$
$$g_{14} = 39.4 \times 10^{-3}\ \mathrm{V\,m/N}, \quad g_{31} = g_{32} = -11.1 \times 10^{-3}\ \mathrm{V\,m/N}, \quad g_{33} = 26.1 \times 10^{-3}\ \mathrm{V\,m/N},$$
$$g_{11} = g_{12} = g_{13} = g_{34} = 0,$$
$$\beta_{11} = 7.66 \times 10^{7}\ \mathrm{V^2/N}, \quad \beta_{33} = 8.69 \times 10^{7}\ \mathrm{V^2/N}, \quad \beta_{13} = 0,$$
$$\alpha_1 = \alpha_2 = 1.923 \times 10^{-6}\ \mathrm{K^{-1}}, \quad \alpha_3 = 0.9355 \times 10^{-6}\ \mathrm{K^{-1}}, \quad \alpha_4 = 0,$$
$$\lambda_3 = 3474.8\ \mathrm{N\,C^{-1}\,K^{-1}}, \quad \lambda_1 = 0$$

The values of k_{ij} are assumed to be the same as PZT-5H because they cannot found in the existing literature.

Graphite-epoxy with fiber orientation along z-axis (Wang and Crossman, 1977):

$$E_z = 137.9\ \mathrm{GPa}, \quad E_x = E_y = 14.48\ \mathrm{GPa}, \quad v_{xy} = v_{zx} = v_{zy} = 0.21,$$
$$G_{xy} = G_{xz} = G_{yz} = 5.86\ \mathrm{GPa}$$

No thermal properties of graphite-epoxy can be found in Wang and Crossman (1977). In this paper, the typical values of the thermal properties

$$\alpha_1 = \alpha_2 = 0.02 \times 10^{-6}\ \mathrm{K}^{-1}, \quad \alpha_3 = 20 \times 10^{-6}\ \mathrm{K}^{-1}, \quad \alpha_4 = 0,$$

$$k_{11} = 1\ \mathrm{W\,K^{-1}\,m^{-1}}, \quad k_{33} = 5\ \mathrm{W\,K^{-1}\,m^{-1}}, \quad k_{13} = 0$$

are assumed. No electrical property is required because the graphite-epoxy is considered as a perfectly electric insulated body. The traditional Lekhnitskii formulation (Lekhnitskii, 1963) can be applied to the graphite-epoxy.

The poling of the selected PZT's and the fiber of the graphite-epoxy lie in the x–z plane and make an angle β with the z-axis (see Fig. 2). For an arbitrary material orientation, the coordinate transformation of the material constants must be made.

Table 1
The stress singularity orders $(-s-2)$ of the isotropic bonded wedges

Wedge descriptions	Mat 1: $E = 300$ GPa, $v = 0.3$ Mat 2: $E = 100$ GPa, $v = 0.3$ $\theta_1 = 0°$, $\theta_2 = 135°$, $\theta_2 = -90°$	Mat 1: $E = 300$ GPa, $v = 0.2$ Mat 2: $E = 50$ GPa, $v = 0.3$ $\theta_1 = 0°$, $\theta_2 = 150°$, $\theta_2 = -165°$
Present	−0.309215	−0.441223 + 0.037182i
Theocaris (1974)	−0.309215	−0.441223 + 0.037182i

Table 2
The stress singularity orders $(-s-2)$ of the graphite-epoxy bonded wedges

Wedge angle	$\theta_1 = 0°$, $\theta_2 = 90°$, $\theta_3 = 180°$	$\theta_1 = 0°$, $\theta_2 = 180°$, $\theta_3 = 180°$
Fiber orientation	$\beta_1 = 45°$ $\beta_2 = -45°$	$\beta_1 = 0°$ $\beta_2 = 90°$
Present	−0.494309 −0.0214846	−0.5
Chue and Liu (2001)	−0.494309 −0.0214846	−0.5

Table 3
The stress singularity orders $(-s-2)$ of the piezoelectric/piezoelectric and graphite-epoxy/piezoelectric bonded wedges

Wedge type	PZT-4/PZT-4 (crack in one material)	PZT-5H/PZT-4	Gr.-Ep./PZT-4	Gr.-Ep./PZT-4
Wedge angle	$\theta_1 = 0°$, $\theta_2 = 180°$, $\theta_3 = 180°$	$\theta_1 = 0°$, $\theta_2 = 90°$, $\theta_3 = 180°$	$\theta_1 = 0°$, $\theta_2 = 180°$, $\theta_3 = 180°$	$\theta_1 = 90°$, $\theta_2 = 180°$, $\theta_3 = 180°$
Poling or fiber orientation	$\beta_1 = 0°$ $\beta_2 = 0°$	$\beta_1 = 0°$ $\beta_2 = 180°$	$\beta_1 = 90°$ $\beta_2 = 180°$	$\beta_1 = 90°$ $\beta_2 = 180°$
Present	−0.5	−0.537789 −0.291115 −0.142352	−0.5 + 0.0451570i	−0.479321 −0.358844 + 0.0231108i
Chue and Chen (2002)	−0.5	−0.537789 −0.291115 −0.142352	−0.5 + 0.0451570i	−0.479321 −0.358844 + 0.0231108i

In this section, all the numerical results are computed from the specific temperature field of Eq. (46). It has been shown that the singularity orders and angular functions of an elastic bonded wedge are independent of the temperature field (Yang and Munz, 1994; Ma, 1995). Based on the present formulation, a numerical examination reveals that the same conclusion can be made for a piezoelectric bonded wedge.

By letting the piezoelectric constants be zero, the present work can be decoupled into elasticity and electrostatics (Chue and Chen, 2002). The stress singularity orders of the decoupled problems are compared with some selected isotropic and anisotropic elastic material wedges, which have been widely investigated in the past (Theocaris, 1974; Chen and Nisitani, 1992; Chue and Liu, 2001).

Table 1 lists the stress singularity orders of two isotropic bonded wedges. The perturbation method of Young's modulus is used to simulate an isotropic material (Lin and Hartmann, 1989). The stress singularity orders obtained by the present approach and in Theocaris (1974) are exactly the same. The associated

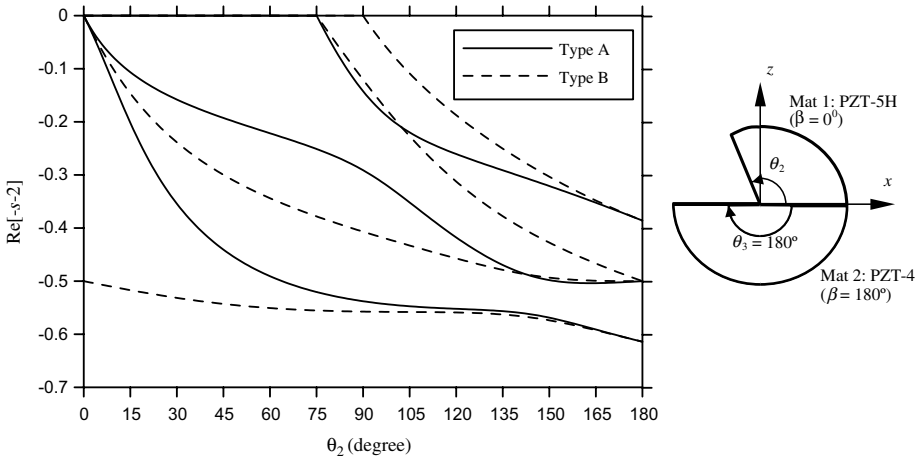

Fig. 5. The variations of the singularity orders $(-s-2)$ of a PZT-5H wedge bonded to a PZT-4 half plane. The poling of the PZT-5H and PZT-4 are along z- and -z-axes, respectively.

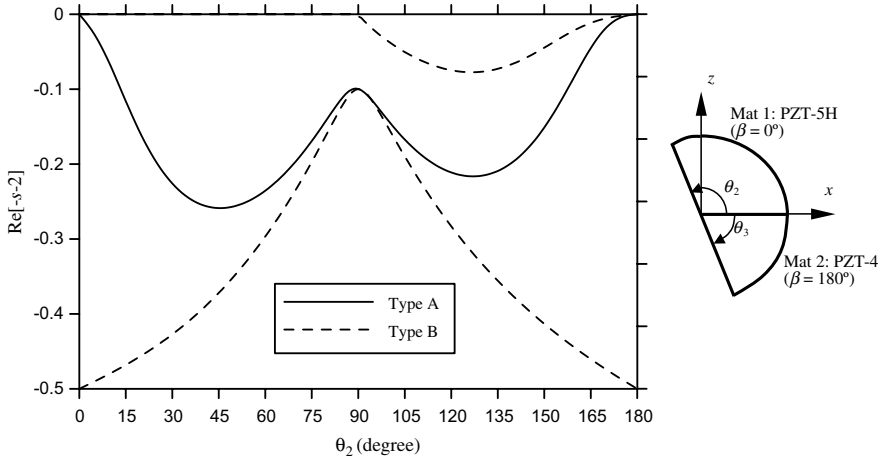

Fig. 6. The variations of the singularity orders $(-s-2)$ of a half plane composed of PZT-5H and PZT-4 wedges.

angular functions of the isotropic bonded wedges listed in Table 1 can be also obtained by the present approach. Chen and Nisitani (1992) used the complex potential function conjunction with the eigenfunction expansion method to obtain the angular function of an isotropic bonded wedge. Numerical verification of the computed angular functions has also been made by comparing the results obtained by Chen and Nisitani (1992).

For the anisotropic wedge, the cases compared are listed in Table 2. The computed stress singularity orders of these wedges are exactly the same as those obtained from Chue and Liu (2001).

Chue and Chen (2002) used the generalized Lekhnitskii formulation to obtain the singularity orders of the piezoelectric and graphite-epoxy/piezoelectric bonded wedges for type A continuity conditions. The cases compared between Chue and Chen (2002) and the present results for the piezoelectric bonded wedges are listed in Table 3.

The consistent results from these reduced cases provide a good reason to trust the validity of the present approach. What follows are some new findings about the singularities of the piezoelectric bonded wedge.

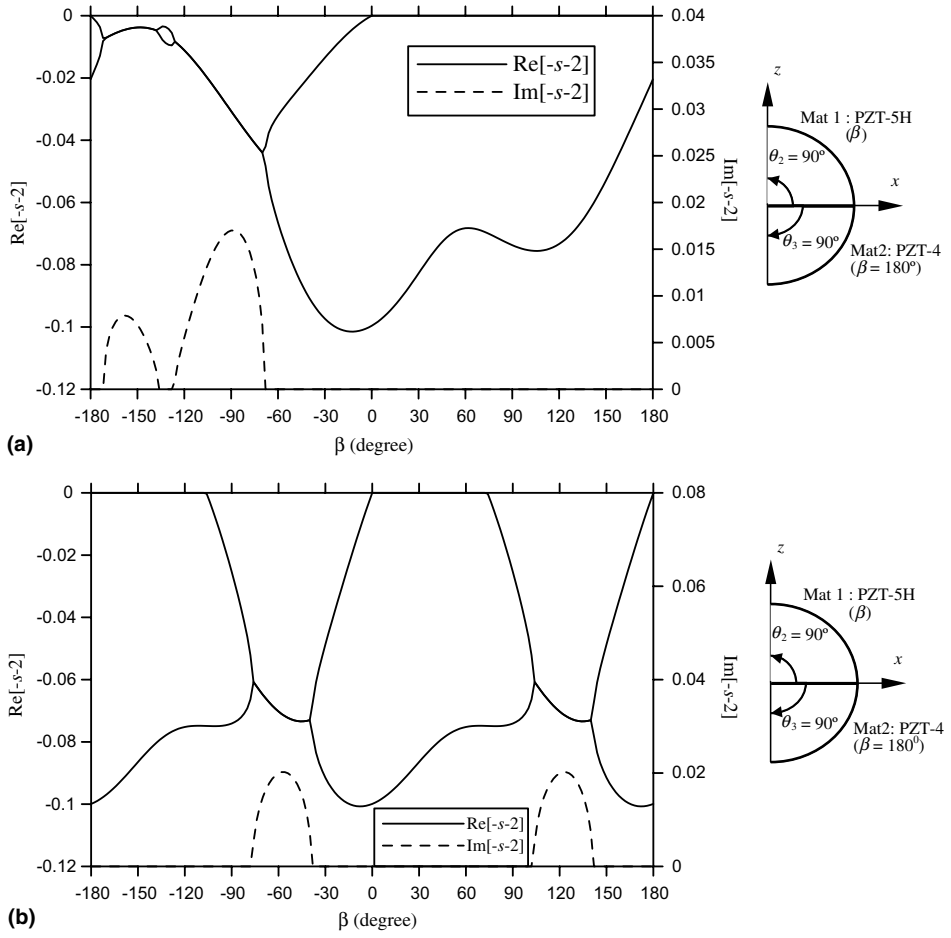

Fig. 7. The variations of the singularity orders $(-s-2)$ of two right-angle bonded wedges composed of PZT-5H and PZT-4 for (a) type A and (b) type B.

6.1. PZT-5H/PZT-4 bonded wedge

Consider a PZT-5H wedge bonded to a PZT-4 half plane. The poling of the PZT-5H and PZT-4 are along z- and $-z$-axes, respectively. The wedge angles are $\theta_1 = 0$, $\theta_3 = 180°$ and θ_2 is a variable which ranges from 0° to 180°. Fig. 5 plots the singularity orders $(-s-2)$ for type A and type B continuity conditions. Chue and Liu (2001) have shown that for a crack existing at the interface between two anisotropic materials, the singularity order is complex and its real part is -0.5. In Fig. 5, the wedge becomes a crack existing at the interface between two materials when $\theta_2 = 180°$. The singularity orders are -0.614073, -0.5 and -0.385927 for both types of continuity conditions. No complex order is found when $\theta_2 = 180°$. It should be noted that this conclusion does not hold for every type of piezoelectric bonded wedge for $\theta_2 = 180°$. For example, if the elastic constant s_{11} of PZT-5H is magnified to 150×10^{-12} m^2 N and the other material constants remain unchanged, the singularity orders for type A and B become $-0.5 + 0.0454004$i and -0.5, respectively. Some researchers, such as Chue and Liu (2001); Scherzer and Kuna (2004), and Govorukha and Kamlah (2004), have found that for a crack existing at the interface between two materials, the singularity order is $-0.5 + i\epsilon$, where ϵ is a real number. These findings are the same as the present results. When $\theta_2 = 0°$, the wedge becomes a PZT-4 half plane. For type A continuity conditions there would be no singularity. However, for type B, there is a -0.5 singularity. This phenomenon results from the assumptions made about the boundary edges and interface, i.e. electrically insulated on the free edge and electrically grounded on the interface. The apex of the wedge becomes a mixed boundary value problem of the electrostatics and the singularity order is -0.5. The order resulting from the mixed point is always stronger than -0.5 for every θ_2.

Fig. 6 plots the singularity orders of a half plane consisting of PZT-5H and PZT-4 wedges. In this example, $\theta_2 + \theta_3 = 180°$ and $\theta_1 = 0$. The poling of the PZT-5H and PZT-4 is along z- and $-z$-axes, respectively. When $\theta_2 = 0$ or $\theta_3 = 0$, the wedge becomes a half plane and the singularity order is 0 for type A continuity conditions and -0.5 for type B. The first order for type B is always greater than that for type A.

Consider a PZT-5H/PZT-4 wedge bonded to form a half plane with wedge angles $\theta_2 = \theta_3 = 90°$ and $\theta_1 = 0$. The poling of PZT-4 is along $-z$ axis. Fig. 7 shows the variations of $(-s-2)$ under different poling direction β of PZT-5H. For type B continuity conditions, the singularity orders are the same as under poling directions β and $(\beta + 180°)$, i.e., opposite poling directions. The reoccurrence of singularity orders results from the electrically grounded condition at the interface. When the poling direction is reversed, the

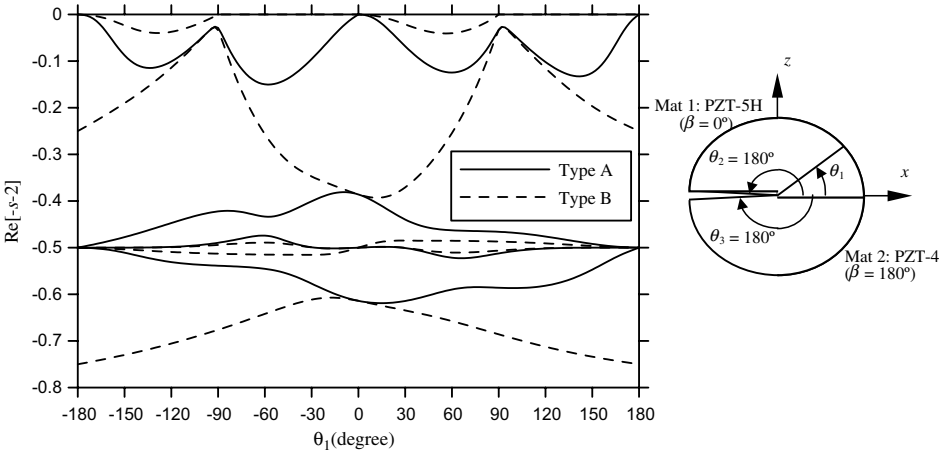

Fig. 8. The variations of the singularity orders $(-s-2)$ of a debonded PZT-5H/PZT-4 junction with wedge angles $\theta_2 = \theta_3 = 180°$.

elastic constants s_{ij} and impermittivities β_{ij} remain unchanged and the piezoelectric constants g_{ij} change by multiplying -1. The singularity orders of type A in Fig. 7 are weaker than those in Fig. 6. For type B, $\mathrm{Re}[-s-2]$ is weaker than -0.1 for most β. Since both the two materials are right-angle-wedges, the phenomenon that $\mathrm{Re}[-s-2]=-0.5$ is not found for type B. The complex orders for both types are found for some β.

Consider a debonded PZT-5H/PZT-4 junction with wedge angles $\theta_2=\theta_3=180°$. The orientation of the interface can be arbitrary. The poling orientation angles β of the PZT-5H and PZT-4 are 0° and 180°, respectively. The variations of singularity orders $(-s-2)$ versus θ_1 are shown in Fig. 8. In the case of type A continuity conditions, the debonded junction can be considered as a crack existing in one material with traction free and electrically open boundary conditions at the crack faces when $\theta_1=-180°$ or 180° and the order is -0.5. For $\theta_1\neq\pm180°$, the first order is always stronger than -0.5. For $\theta_1=0$, the wedge becomes a crack existing at the interface between two half planes and the orders are -0.38593, -0.5 and -0.61407. In the case of type B, the singularity orders are -0.75, -0.5 and -0.25 when $\theta_1=-180°$ or 180°. For such θ_1 the electrical boundary conditions are electrically grounded and insulated at the crack faces. The singu-

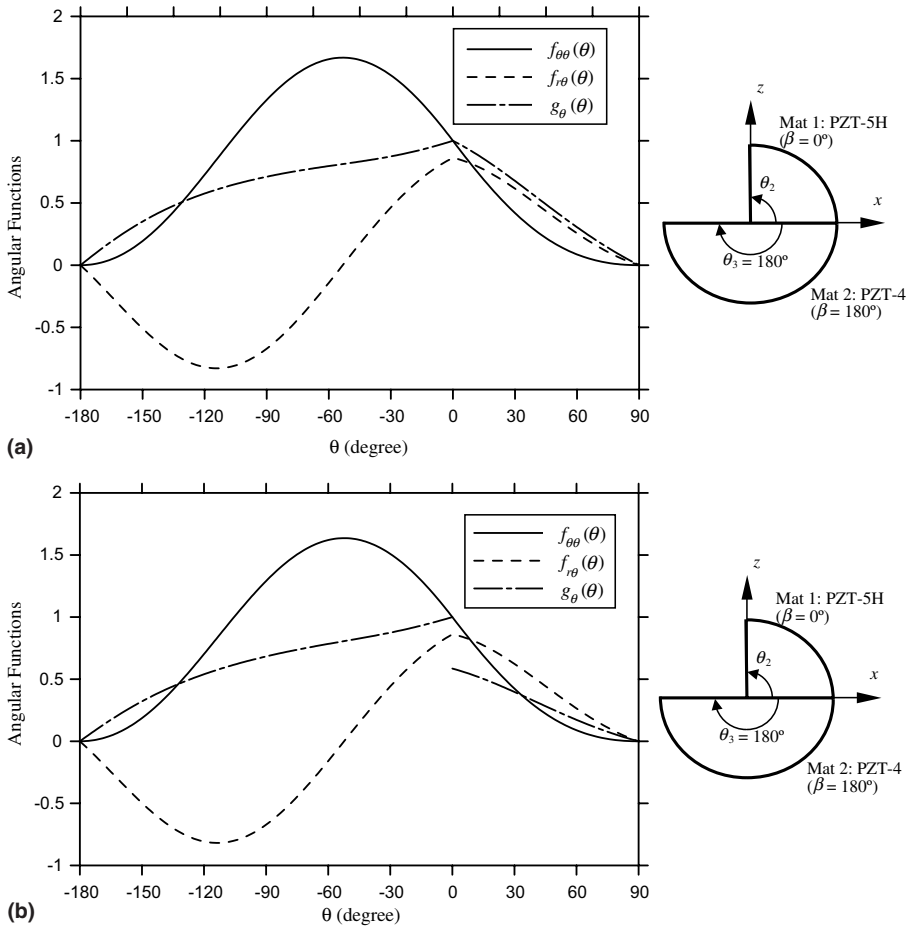

Fig. 9. The variations of the angular functions corresponding to the strongest order of a right-angle PZT-5H wedge bonded to a PZT-4 half plane for (a) type A ($-s-2=-0.537789$) and (b) type B ($-s-2=-0.557356$). The poling orientation angles β of PZT-5H and PZT-4 are 0° and 180°, respectively.

larity orders for $\theta_1 = -180°$ or 180° are exactly the same as the crack problem in one elastic material when clamped and traction free at the crack faces. For $\theta_1 = 0$, the orders are −0.38592, −0.5 and −0.61408, which are slightly different from type A under the same θ_1 The first order for type B is always stronger than that for type A. Furthermore, no complex order is found for either type.

Consider a right-angle PZT-5H wedge bonded to a PZT-4 half plane. The poling orientation angles β of PZT-5H and PZT-4 are 0° and 180°, respectively. The singularity orders of this piezoelectric bonded wedge are −0.537789, −0.291115, −0.142352 for type A and −0.557356, −0.406894, −0.120547 for type B. The angular functions of the piezoelectric bonded wedge can be computed numerically. Fig. 9 shows the angular functions corresponding to the strongest order. It is observed that all the angular functions are continuous across the interface and vanish at the boundary edges except $g_\theta(\theta)$ at the interface for type B.

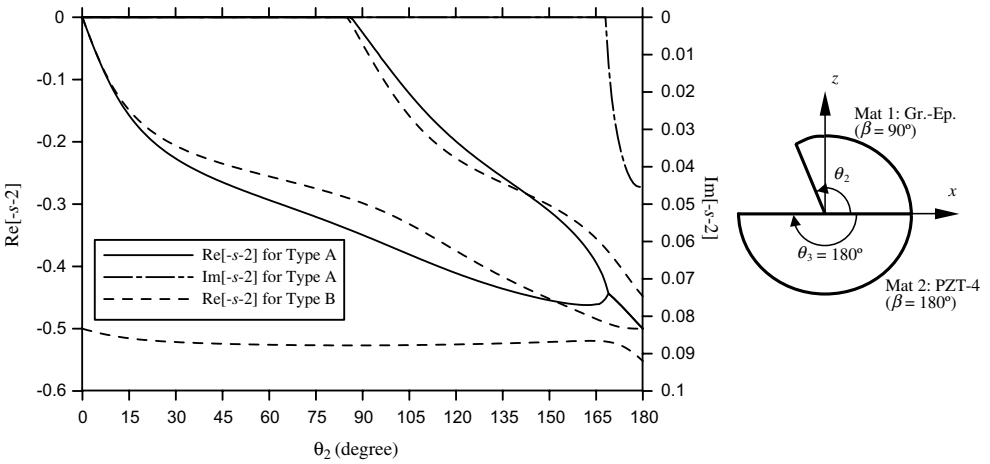

Fig. 10. The variations of the singularity orders $(-s-2)$ of a graphite-epoxy wedge bonded to a PZT-4 half plane. The material orientation angles β of graphite-epoxy and PZT-4 are 90° and 180°, respectively.

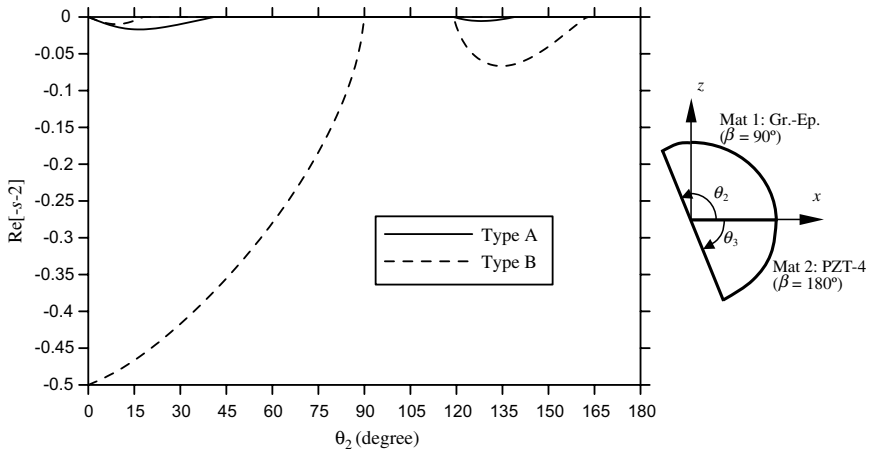

Fig. 11. The variations of the singularity orders $(-s-2)$ of a half plane composed of graphite-epoxy and PZT-4 wedges. The material orientation β of graphite-epoxy and PZT-4 are 90° and 180°, respectively.

6.2. Graphite-epoxy/PZT-4 bonded wedge

Consider a graphite-epoxy wedge bonded to PZT-4 half plane as shown in Fig. 10. The x-axis is placed along the interface ($\theta_1 = 0$) and the wedge angle of PZT-4 is $\theta_3 = 180°$. The material orientations of the graphite-epoxy and PZT-4 are along x and $-z$-axes, respectively. The wedge angle θ_2 is a variable that ranges from 0° to 180°. For type A, a complex order is found when θ_2 approaches 180°. Chue and Chen (2002) have studied type A continuity conditions for this example. There are some slight differences in the material properties of the graphite-epoxy between Chue and Chen (2002) and this paper. The overall tendencies of the two studies are the same. For type B, no complex order is found and there exists an order stronger than -0.5 for every possible θ_2. Again this phenomenon results from the mixed point of the electrical boundary conditions.

Fig. 11 shows the singularity orders of a half plane consisting of graphite-epoxy and PZT-4 wedges. The x-axis is placed along the interface and $\theta_2 + \theta_3 = 180°$. The material orientation angles β of graphite-epoxy and PZT-4 are 90° and 180°, respectively. For type A, the singularity order is always weaker than -0.017

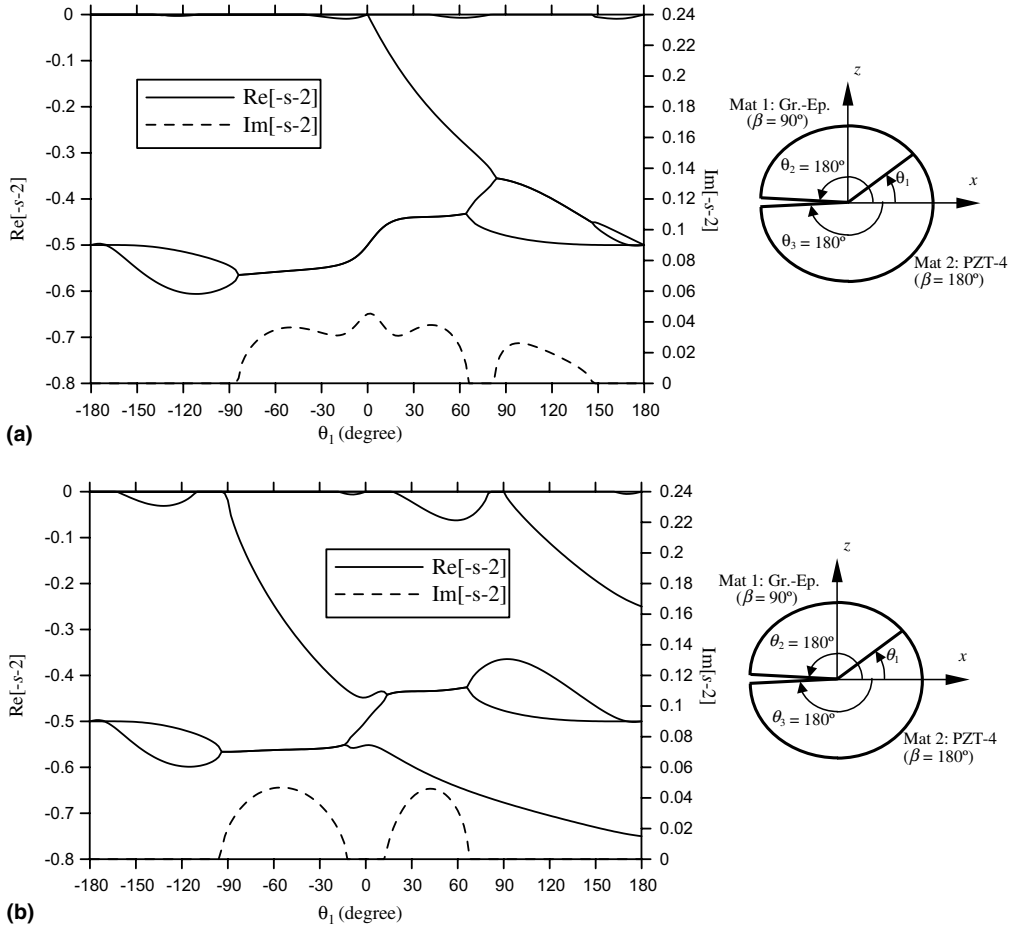

Fig. 12. The variations of the singularity orders ($-s-2$) of a debonded graphite-epoxy/PZT-4 junction for (a) type A and (b) type B. The material directions of the graphite-epoxy and PZT-4 are along x- and -z-axes, respectively.

and disappearance of the singularity is observed for $180° > \theta_2 > 139°$ and $119° > \theta_2 > 42°$. For type B, the regions of disappearance of the singularity are $180° > \theta_2 > 163°$ and $119° > \theta_2 > 90°$. When $\theta_2 < 90°$, an order due to mixed point is found. When $\theta_2 = 0$, the order becomes -0.5. Contrary to Fig. 6, the phenomenon of the mixed point does not occur when $\theta_2 > 90°$ because the electrostatic properties of graphite-epoxy are ignored, i.e., graphite-epoxy is modeled as a perfectly electric insulated body.

Consider a debonded graphite-epoxy/PZT-4 junction with wedge angle $\theta_2 = \theta_3 = 180°$ and $180° > \theta_1 > -180°$. The material directions of the graphite-epoxy and PZT-4 are along the x and $-z$-axes, respectively. The variation of the singularity orders are shown in Fig. 12. Chue and Chen (2002) have studies a similar wedge for type A boundary conditions. In Chue and Chen's study, the fiber of the graphite-epoxy is parallel to the bonded surface while the poling of PZT-4 is perpendicular to the bonded surface. Although there are some differences between these two studies, the overall tendencies are quite similar. It is concluded that if the wedge angle of the graphite-epoxy is smaller than that of the PZT-4, the singularity order would be weaker.

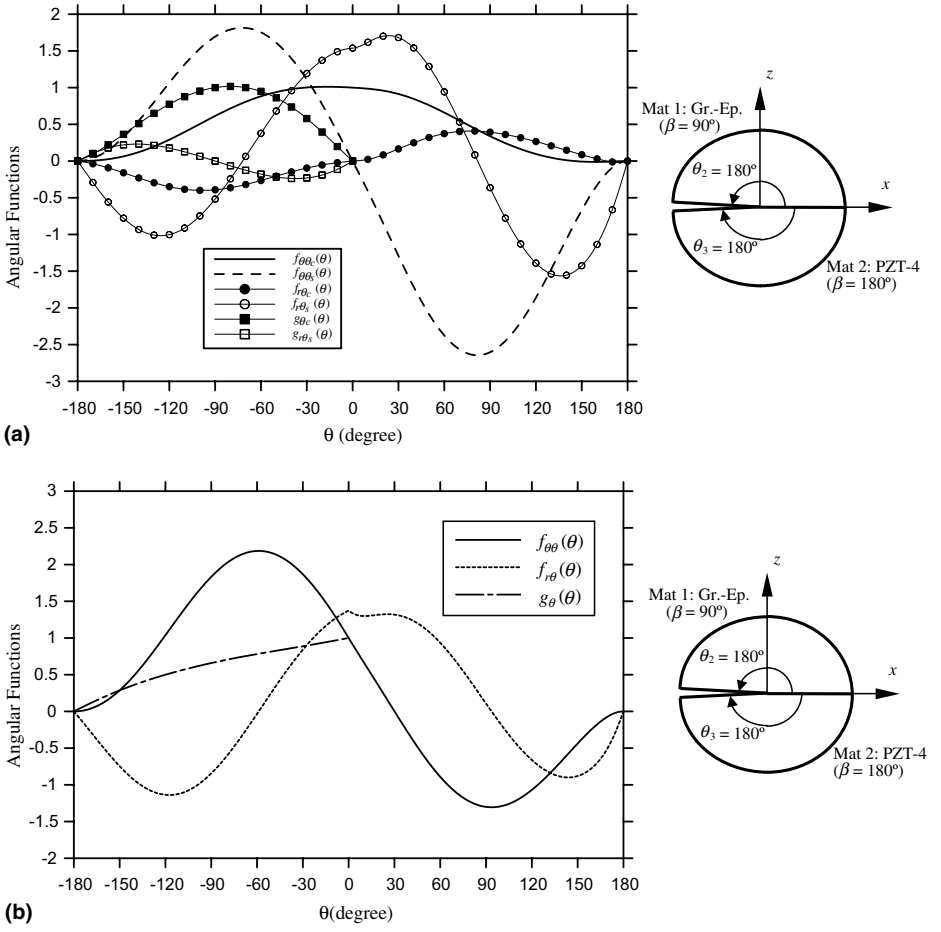

Fig. 13. The variations of the angular functions corresponding to the strongest order of a debonded graphite-epoxy/PZT-4 junction for (a) type A ($-s-2 = -1.5 + 0.451570$i) and (b) type B ($-s-2 = -0.551993$). The material orientation angles β of graphite-epoxy and PZT-4 are 90° and 180°.

In Fig. 12, there are three orders when $\theta_1 = 180°$ for type B. When $\theta_1 = 0$, there is only one order -0.5. For all possible θ_1 the first singularity order is always stronger than -0.5. The strongest order is -0.75 when $\theta_1 = 180°$. In addition, if the wedge angle of graphite-epoxy is smaller than PZT-4, the singularity order would be stronger, which is contrary to type A.

Consider a crack existing at the interface of the graphite-epoxy and PZT-4 half planes. The material orientation angles β of the graphite-epoxy and PZT-4 are 90° and 180°, respectively. The wedge angles are $\theta_1 = 0°$ and $\theta_2 = \theta_3 = 180°$. The computed singularity orders of the debonded graphite-epoxy/PZT-4 junction are $-0.5 + 0.451570i$ for type A and -0.551993, -0.5, -0.448007 for type B. Fig. 13 shows the angular functions corresponding to the first order of the debonded graphite-epoxy/PZT-4 junction. Since the graphite-epoxy is considered as a perfectly electric insulated body, there is no angular function of electric displacement inside it. Similar to Fig. 9, all the angular functions vanish at the boundary edges in Fig. 13. The angular functions of stresses and electric displacements are continuous across the interface for type A. For type B, the angular function of electric displacement has a jump across the interface.

7. Conclusions

In this paper, the thermo-electro-elastic fields of a piezoelectric bonded wedge have been analyzed by the generalized Lekhnitskii formulation conjunction with the Mellin transform. Based on the potential theory for the wedge-shaped region, the general form of the temperature change has been presented as the particular solution of the Lekhnitskii formulation.

The boundary edges of the wedge are traction free and electrically insulated. Two types of continuity conditions, namely type A and type B have been investigated in this study. From the inversion of the Mellin transform, the singularity orders of the wedge have been computed numerically through solving the poles of the transformed electro-elastic fields. The angular functions are also computed numerically. Compared with type A, the type B condition may induce an order stronger than -0.5 due to the mixed boundary value problem of the electrostatics. The results of this study provide a guide to the reduction or even disappearance of the singularity in the piezoelectric wedges.

References

Berlincourt, D.A., Curran, D.R., Jaffe, H., 1964. Piezoelectric and piezoceramic materials and their function in transducers. In: Mason, W.P. (Ed.), Physical Acoustics, vol. I-A. Academic Press, New York.

Bogy, D.B., 1968. Edge-bonded dissimilar orthogonal elastic wedges under normal and shear loading. Journal of Applied Mechanics 35, 460–466.

Bogy, D.B., 1972. The plane solution for anisotropic elastic wedge under normal and shear loading. Journal of Applied Mechanics 39, 1103–1109.

Chen, C.D., Chue, C.H., 2003. Singular electro-mechanical fields near the apex of a piezoelectric bonded wedge under antiplane shear. International Journal of Solids and Structures 40, 6513–6526.

Chen, D.H., Nisitani, H., 1992. Singular stress field in two bonded wedges. Transactions of Japan Society of Mechanical Engineers, Series A 58, 457–464.

Chen, H.P., 1998. Stress singularities in anisotropic multi-material wedges and junctions. International Journal of Solids and Structures 35, 1057–1073.

Chue, C.H., Chen, C.D., 2002. Decoupled formulation of piezoelectric elasticity under generalized plane deformation and its application to wedge problems. International Journal of Solids and Structures 39, 3131–3158.

Chue, C.H., Chen, C.D., 2003. Antiplane stress singularities in a bonded bimaterial piezoelectric wedge. Archive of Applied Mechanics 72, 673–685.

Chue, C.H., Liu, C.I., 2001. A general solution on stress singularities in anisotropic wedge. International Journal of Solids and Structures 38, 6889–6906.

Delale, F., 1984. Stress singularities in bonded anisotropic materials. International Journal of Solids and Structures 20, 31–40.

Ding, H.J., Wang, H.M., Ling, D.S., 2003. Analytical solution of a pyroelectric hollow cylinder for piezothermoelastic axisymmetric dynamic problems. Journal of Thermal Stresses 26, 261–276.

Govorukha, V., Kamlah, M., 2004. Asymptotic fields in the finite element analysis of electrically permeable interface cracks in piezoelectric bimaterials. Archive of Applied Mechanics 74, 92–101.

Lekhnitskii, S.G., 1963. Theory of Elasticity of an Anisotropic Elastic Body. Holden-Day, San Francisco.

Lin, K., Hartmann, H.H., 1989. Numerical analysis of stress singularities at a bonded anisotropic wedge. Engineering Fracture Mechanics 32, 211–224.

Lu, P., Tan, M.J., Liew, K.M., 1998. Piezothermoelastic analysis of a piezoelectric material with an elliptic cavity under uniform heat flow. Archive of Applied Mechanics 68, 719–733.

Ma, C.C., 1995. Plane solution of thermal stresses for anisotropic bimaterial elastic wedges. Journal of Thermal Stresses 18, 219–245.

Ma, C.C., Hour, B.L., 1989. Analysis of dissimilar anisotropic wedge subjected to antiplane shear deformation. International Journal of Solids and Structures 25, 1295–1309.

Niraula, O.P., Noda, N., 2002. Thermal stress analysis in thermopiezoelectric strip with an edge crack. Journal of Thermal Stresses 25, 389–405.

Qin, Q.H., 2001. Fracture Mechanics of Piezoelectric Materials. WIT-Press, Southampton, Boston.

Qin, Q.H., Mai, Y.W., 1999. A closed crack tip model for interface crack in thermopiezoelectric materials. International Journal of Solids and Structures 36, 2463–2479.

Scherzer, M., Kuna, M., 2004. Combined analytical and numerical solution of 2D interface corner configuration between dissimilar piezoelectric materials. International Journal of Fracture 127, 61–99.

Shang, F., Kuna, M., 2003. Thermal stress around a penny-shaped crack in a thermopiezoelectric solid. Computational Materials Science 26, 197–201.

Shang, F., Kuna, M., Scherzer, M., 2002. Analytical solutions for two penny-shaped crack problems in thermopiezoelectric materials and their finite element comparison. International Journal of Fracture 117, 113–128.

Shang, F., Kuna, M., Kitamura, T., 2003. Theoretical investigations of an elliptical crack in thermopiezoelectric material. Part I: Analytical development. Theoretical and Applied Fracture Mechanics 40, 237–246.

Theocaris, P.S., 1974. The order of singularity at a multi-wedge corner of a composite plate. International Journal of Engineering Science 12, 107–120.

Uchino, K., 1997. Piezoelectric Actuators and Ultrasonic Motors. Kluwer Academic Publishers, Norwell Massachusetts.

Wang, A.S.D., Crossman, F.W., 1977. Some new results on edge effect in symmetric composite laminates. Journal of Composite Materials 11, 92–106.

Williams, M.L., 1952. Stress singularities resulting from various boundary conditions in angular corners of plates in tension. Journal of Applied Mechanics 19, 526–528.

Xu, X.L., Rajapakse, R.K.N.D., 2000. On singularities in composite piezoelectric wedges and junctions. International Journal of Solids and Structures 37, 3253–3275.

Yang, Y.Y., Munz, D., 1994. Determination of the regular stress term in a dissimilar materials joint under thermal loading by the Mellin transform. Journal of Thermal Stresses 17, 321–336.

Yu, S.W., Qin, Q.H., 1996. Damage analysis of thermopiezoelectric properties: Part I—crack tip singularities. Theoretical and Applied Fracture Mechanics 25, 737–750.